Experimental Eye Research 212 (2021) 108801

Contents lists available at ScienceDirect

Experimental Eye Research

journal homepage: www.elsevier.com/locate/yexer

Decreased endostatin in db/db retinas is associated with optic disc intravitreal vascularization

Aina Bonet [a,b], Andreia Valença [c,d], Luísa Mendes-Jorge [d,e], Alba Casellas [a,f,g], Alfonso Rodríguez-Baeza [h], Víctor Nacher [a,b,g], David Ramos [a,d], Judit Pampalona [a], Rafael Simó [g,i], Jesús Ruberte [a,b,g,*]

[a] Centre for Animal Biotechnology and Gene Therapy (CBATEG), Universitat Autònoma de Barcelona, Bellaterra, Spain
[b] Department of Animal Health and Anatomy, Faculty of Veterinary Medicine, Universitat Autònoma de Barcelona, Bellaterra, Spain
[c] Faculty of Veterinary Medicine, Universidade Lusófona de Humanidades e Tecnologias, Lisbon, Portugal
[d] Centre for Interdisciplinary Research in Animal Health (CIISA), Faculty of Veterinary Medicine, Universidade de Lisboa, Lisbon, Portugal
[e] Department of Morphology and Function, Faculty of Veterinary Medicine, Universidade de Lisboa, Lisbon, Portugal
[f] Department of Biochemistry and Molecular Biology, Faculty of Veterinary Medicine, Universitat Autònoma de Barcelona, Bellaterra, Spain
[g] Centro de Investigación Biomédica en Red de Diabetes y Enfermedades Metabólicas Asociadas (CIBERDEM), Instituto de Salud Carlos III, Madrid, Spain
[h] Department of Morphological Sciences, Faculty of Medicine, Universitat Autònoma de Barcelona, Bellaterra, Spain
[i] Diabetes and Metabolism Research Unit, Vall d'Hebron Research Institute, Universitat Autònoma de Barcelona, Barcelona, Spain

ARTICLE INFO

Keywords:
Endostatin
Intravitreal vessels
Diabetic retinopathy
db/db mice

ABSTRACT

Endostatin, a naturally cleaved fragment of type XVIII collagen with antiangiogenic activity, has been involved in the regulation of neovascularization during diabetic retinopathy. Here, the intracellular distribution of endostatin in healthy mouse and human neuroretinas has been analyzed. In addition, to study the effect of experimental hyperglycemia on retinal endostatin, the db/db mouse model has been used. Endostatin protein expression in mouse and human retinas was studied by immunofluorescence and Western blot, and compared with db/db mice. Eye fundus angiography, histology, and immunofluorescence were used to visualize mouse retinal and intravitreal vessels.

For the first time, our results revealed the presence of endostatin in neurons of mouse and human retinas. Endostatin was mainly expressed in bipolar cells and photoreceptors, in contrast to the optic disc, where endostatin expression was undetectable. Diabetic mice showed a reduction of endostatin in their retinas associated with the appearance of intravitreal vessels at the optic disc in 50% of db/db mice. Intravitreal vessels showed GFAP positive neuroglia sheath, basement membrane thickening by collagen IV deposition, and presence of MMP-2 and MMP-9 in the vascular wall. All together, these results point that decreased retinal endostatin during experimental diabetes is associated with optic disc intravitreal vascularization. Based on their phenotype, these intravitreal vessels could be neovessels. However, it cannot be ruled out the possibility that they may also represent persistent hyaloid vessels.

1. Introduction

Endostatin was first discovered in the laboratory of Judah Folkman in 1997 and described as an inhibitor of angiogenesis in murine hemangioendothelioma cells (O'Reilly et al., 1997). It is a 20 kDa fragment activated by proteolytic cleavage of the C-terminal region of collagen XVIII by cathepsin L, elastases, and matrix metalloproteinases (MMPs) (Ferreras et al., 2000). Several mechanisms by which endostatin can inhibit endothelial cell proliferation, migration, and invasion have been proposed. Endostatin binds the vascular endothelial growth factor (VEGF) receptor KDR/Flk-1 and, thereby, interferes with VEGF signalling leading to the inhibition of proliferation and migration of endothelial cells (Kim et al., 2002). Endostatin can also promote ß-catenin degradation, inducing cell cycle arrest through inhibition of the cyclin-D1 promoter (Hanai et al., 2002). Furthermore, antimigratory effect of endostatin can also be mediated through its binding with a5ß1

* Corresponding author. CBATEG - Center for Animal Biotechnology and Gene Therapy, Autonomous University of Barcelona, C/ de la Vall Morona, 08193, Bellaterra (Cerdanyola del Vallès), Spain.
E-mail address: jesus.ruberte@uab.es (J. Ruberte).

https://doi.org/10.1016/j.exer.2021.108801
Received 22 January 2021; Received in revised form 1 September 2021; Accepted 18 October 2021
Available online 21 October 2021

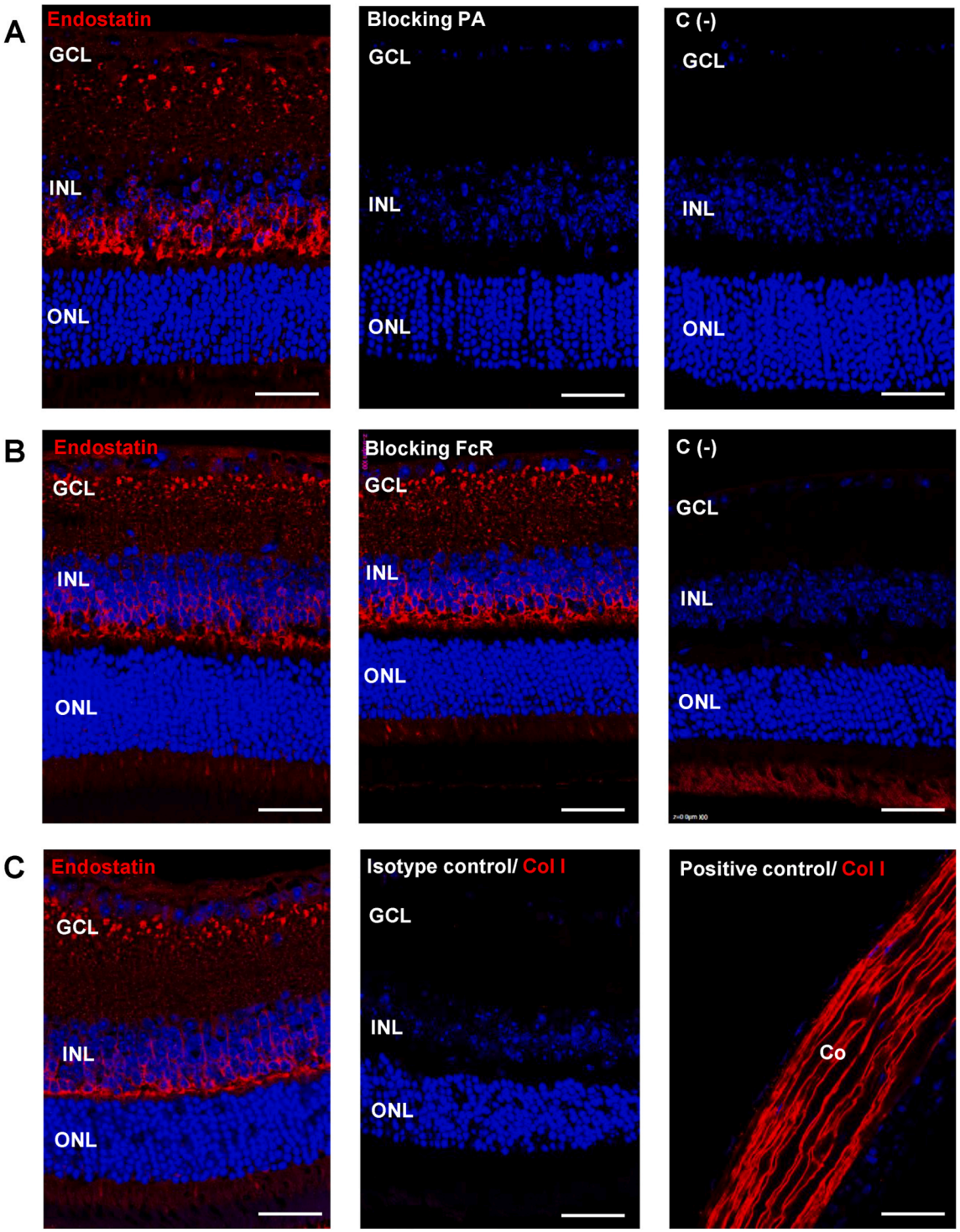

Fig. 1. Endostatin staining and antibody specificity in mouse retina. (**A**) Immunofluorescence with a rabbit polyclonal anti-endostatin antibody in mice retina showed staining in the ganglion cell layer, outer plexiform layer, and in the outer segments of photoreceptors (left panel). Blocking peptide assay (Blocking PA) using recombinant mouse endostatin was performed to assess antibody specificity. Anti-endostatin antibody neutralization was complete and non-specific signal was observed in the retina (middle panel). Negative control was done by omission of the primary antibody (right panel). (**B**) FcR blocking assay confirmed the specificity of endostatin staining (left panel) when compared to retinas incubated with Mouse Seroblock FcR (middle panel). Negative control was done by omission of the primary antibody (right panel). (**C**) Isotype control assay using an anti-collagen I antibody from the same isotype and host as the anti-endostatin antibody was performed. Collagen I is absent from retina and very abundant in cornea. In comparison with the anti-endostatin antibody retinal signal (left panel), non-signal was observed in the retina when using anti-collagen I antibody (middle panel). Positive control for collagen I was performed in the cornea of the same eye in a consecutive section (right panel). Nuclei were counterstained with Hoechst. GCL: ganglion cell layer; INL: inner nuclear layer; ONL: outer nuclear layer; Co: cornea. Scale bars: 37.03 μm.

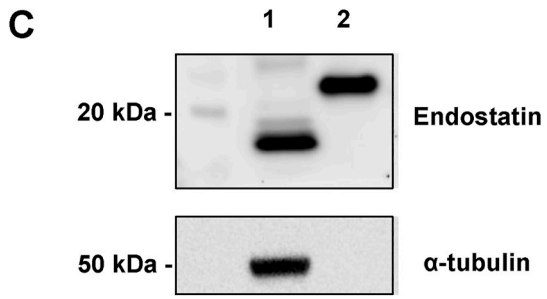

Fig. 2. Western blot analysis of mouse retinal endostatin. Retinal endostatin shows a main band between 15 and 20 kD (lane 1), very close to the 21 kDa band from the recombinant endostatin (lane 2), confirming the antibody specificity for cleaved endostatin. α-tubulin was used as a loading control.

integrin (Wickström et al., 2002) and the inhibition of MMP-2 activity (Kim et al., 2000). MMP-2 regulates angiogenesis by degrading collagens, laminins, and glycosaminoglycans in the blood basement membrane allowing the sprout of new vessels (Waszczykowska et al., 2020).

In mouse and human neuroretinas, endostatin has only been immunolocalized at the internal limiting membrane (Takahashi et al., 2003; Bhutto et al., 2004; Ohlmann et al., 2004; Ramesh et al., 2004; May et al., 2006; Määttä et al., 2007) and at the wall of retinal vessels, including hyaloid vessels (Bhutto et al., 2004; Ohlmann et al., 2004; May et al., 2006; Määttä et al., 2007). It is believed that this staining pattern is due to cross-reactivity between endostatin and its precursor, collagen XVIII (Takahashi et al., 2003), which is a very well known component of basement membranes (Pehrsson et al., 2019). Endostatin is not expressed in neuroectodermal cells during development, (Miosge et al., 2003), however, adult neurons containing endostatin have been found in physiological conditions in human cortex (Deininger et al., 2002). Likewise, increased neuronal deposition of endostatin is found during Alzheimer's disease (Deininger et al., 2002) and cerebral ischemia (Hou et al., 2010). To date, no studies about intraneuronal endostatin in the retina have been reported.

Proliferative diabetic retinopathy is still a leading cause of visual impairment in the working-age population in developed countries (Nawaz et al., 2019). It is characterized by proliferation of fibrovascular tissue formed by the extension of retinal angiogenesis into the vitreous cavity, which ultimately leads to vitreous traction and retinal detachment (Boulton et al., 1988). Prevailing evidence suggests that changes in the relative balance between inducers and inhibitors of angiogenesis may activate the angiogenic switch in the diabetic retina (Simó et al., 2006). The inhibitor of angiogenesis endostatin has been involved in the regulation of neovascularization during diabetic retinopathy. The concentration of endostatin in the vitreous fluid of patients with diabetic retinopathy significantly correlates with the severity of the disease. It

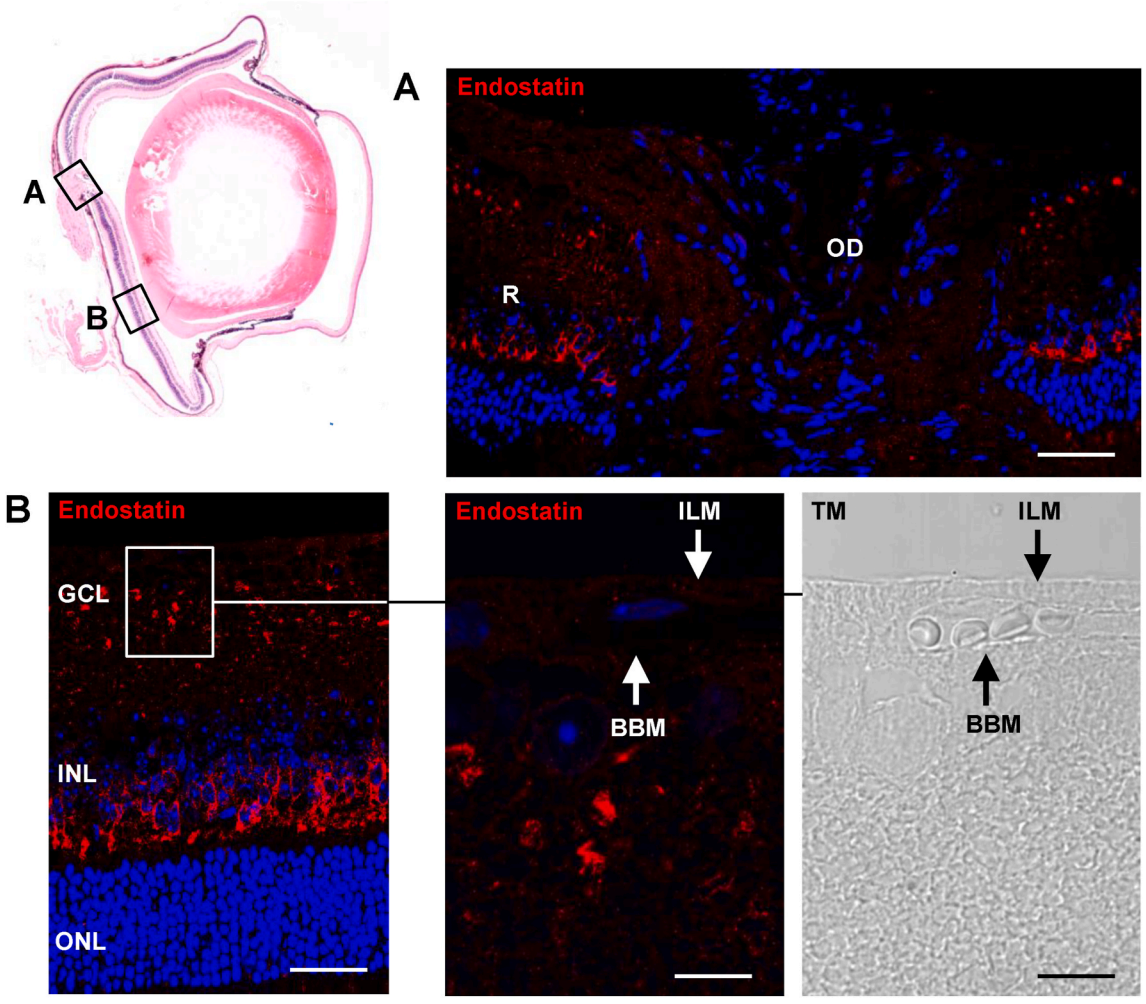

Fig. 3. Endostatin in mouse neuroretina. (**A**) Immunostaining with anti-endostatin antibody revealed that endostatin is accumulated in the inner part of neuroretina, however, it was not observable at the optic disc (**B**) No endostatin signal was detected in blood vessel basement membranes or in the internal limiting membrane. Nuclei were counterstained with Hoechst. GCL: ganglion cell layer; INL: inner nuclear layer; ONL: outer nuclear layer; BBM: blood vessel basement membrane; ILM: internal limiting membrane. Scale bars: 43.48 μm (A); 33.33 μm (B).

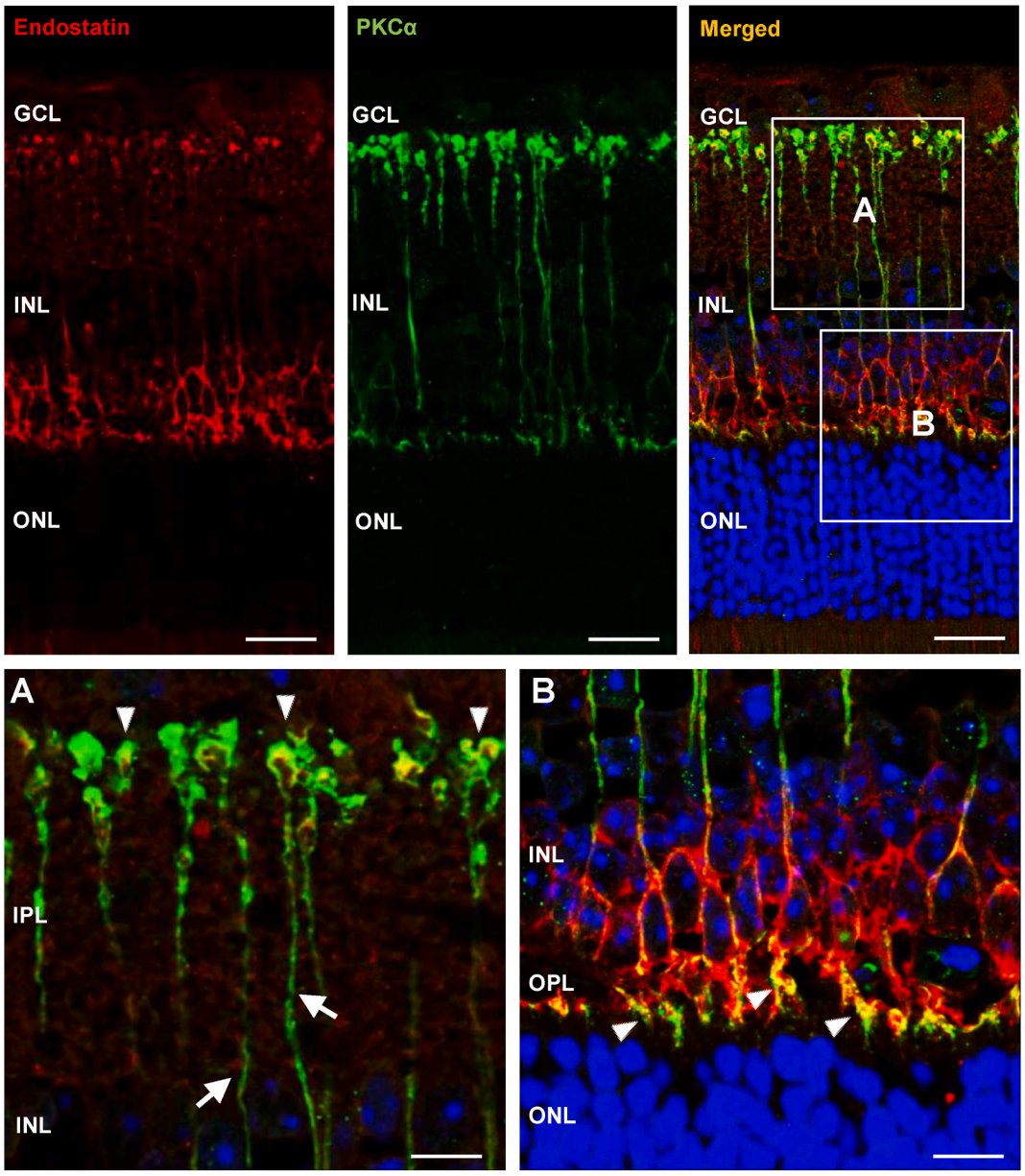

Fig. 4. Endostatin is accumulated in bipolar cells of mouse retina. Double immunostaining with anti-PKCα antibody confirmed that endostatin was accumulated mainly in bipolar cells. Endostatin was found in their axon terminals (arrowheads), but not in their axons themselves (arrows) (**A**) and in the perikaryon and dendrites (arrowheads) (**B**). Nuclei were counterstained with Hoechst. GCL: ganglion cell layer; IPL: inner plexiform layer; INL: inner nuclear layer; OPL: outer plexiform layer; ONL: outer nuclear layer. Scale bar: 25.42 μm; 9.41 μm (A); 10.17 μm (B).

has been shown that eyes with low levels of endostatin and high levels of VEGF in the vitreous have a significantly greater risk of progression to the proliferative phase of diabetic retinopathy (Noma et al., 2002; Funatsu et al., 2003). Furthermore, it has been observed that endostatin in age-related macular degeneration is highly decreased in angiogenic areas of the choroid (Bhutto et al., 2004).

In this study, our results revealed for the first time the presence of intracellular endostatin in neurons of mouse and human retinas. Endostatin distribution was homogeneous throughout the neuroretina except for the optic disc where endostatin was undetectable. Diabetic mice showed a reduction of endostatin in their neuroretinas that was associated with the appearance of intravitreal vessels protruding from the optic disc. Intravitreal vessels phenotype showed similarities to the human diabetic papillovitreal neovessels, suggesting that neovascularization may occur at the optic disc in diabetic mice. However, it cannot be ruled out that the intravitreal vessels in db/db mice may represent persistent hyaloid vessels.

2. Materials and methods

2.1. Human eyes

Human eyes were obtained from voluntary donations to the Faculty of Medicine of the UAB, following the Catalan law (Decret 297/1997) about human samples for research purposes. The procedure was approved by the Ethics Committee in Animal and Human Experimentation of the UAB and carried out in accordance with The Code of Ethics of the World Medical Association (Declaration of Helsinki) for experiments involving humans. Two eyes from two different donors were used in this study. Only biological data (sex, age, brief clinical history and cause of death) were provided. None of them suffered from diabetis *mellitus*. Eyes were fixed in a solution of paraformaldehyde 4% with

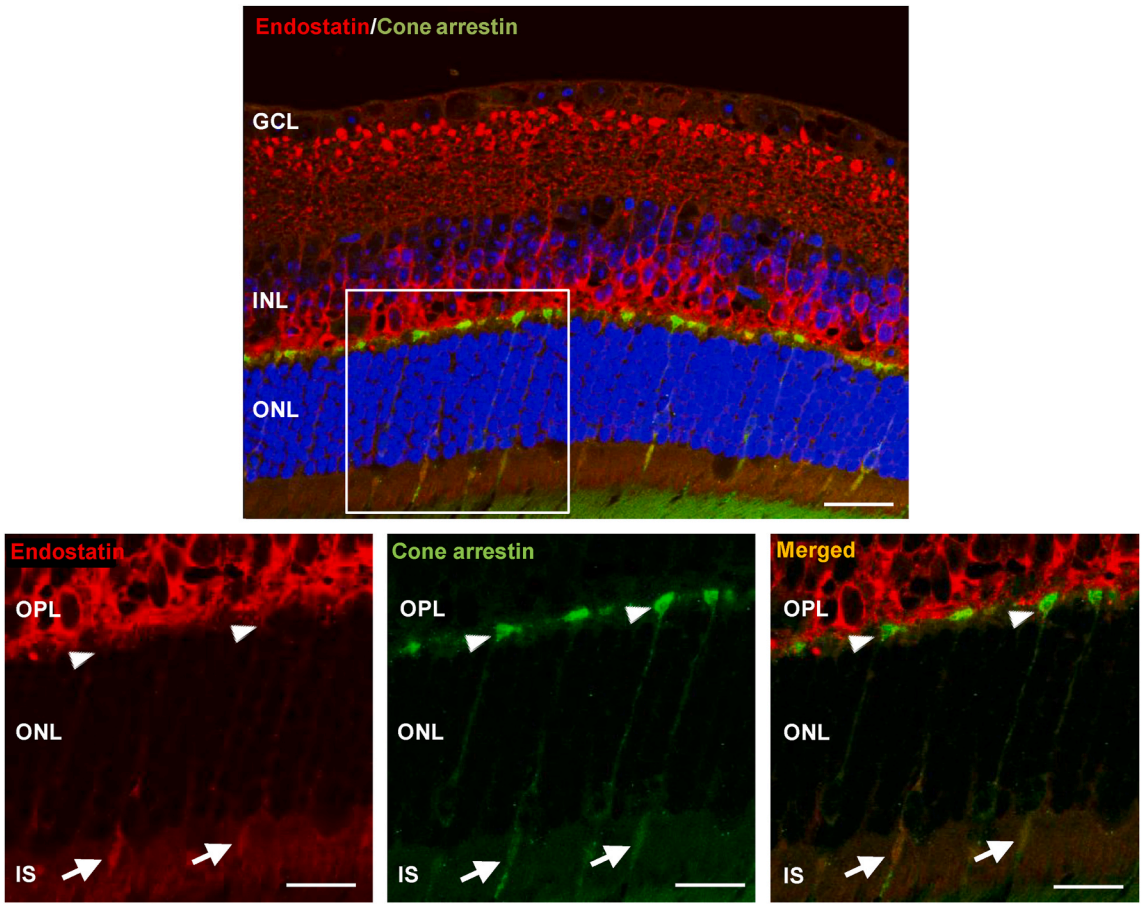

Fig. 5. Endostatin is present in cone photoreceptors of mice retina. Double immunostaining with anti-cone arrestin antibody showed endostatin in the inner segments of cone photoreceptors (arrows). Cone synaptic terminals did not show endostatin expression (arrowheads). Nuclei were counterstained with Hoechst. GCL: ganglion cell layer; INL: inner nuclear layer; OPL: outer plexiform layer; ONL: outer nuclear layer; IS: inner segments of photoreceptors. Scale bar: 25.88 μm; 17.25 μm (inset).

picric acid in 0.01 M PBS for 24 h. After several washes in PBS, the eyes were partially dehydrated, and maintained in a solution of 70% alcohol at 4 °C. For immunohistochemical analysis, 3 μm paraffin retinal sections were used.

2.2. Mice

A total of 14 male diabetic db/db (BKS.Cg-Dock7^{m} +/+ Lepr^{db}/J) and 14 non-diabetic db/+ (BKS.Cg-Dock7^{m} + Lepr^{db}/+) control mice aged 8 and 12 weeks were used in this study. Mice were maintained under controlled conditions (20 °C temperature, 60% humidity and 12 h light/dark cycles) and provided with free access to water and food (2018S TEKLAD Global, Harlan Teklad, Madison, WI, USA).

All mice were euthanized with an overdose of isoflurane inhalation followed by cervical dislocation. Animal care and experimental procedures were permormed according to the ARVO Statement for the Use of Animals in Ohthalmic and Vision Research and Animal care ARRIVE guidelines and were approved by the Ethics Committee in Animal and Human Experimentation of the Universitat Autònoma de Barcelona (UAB) (FUE-2018-00717286).

2.3. Glycemia measurement

Blood was collected from the tail vein every week to monitor glycemia using a glucometer (Bayer, Leverkusen, Germany). Mice were analyzed in non-fasted conditions and were considered diabetic when glycemia exceeded 250 mg/dl in two consecutive measurements. The last measurement was performed before euthanasia. db/db mice develop obesity and hyperglycemia at 4–8 weeks of age, becoming a widely accepted model of diabetes type II (Robinson et al., 2012). In this regard, significant statistical differences were found in 8-week-old mice body weight (25.533 ± 0.383 g in db/+ vs. 36.067 ± 1.144 g in db/db; $p < 0.0001$; $n = 6$) and glycemia (150.167 ± 9.026 mg/dl in db/+ vs. 436.167 ± 14.597 mg/dl in db/db; $p < 0.0001$; $n = 6$) and also in 12-week-old mice body weight (25.65 ± 0.6462 g in db/+ vs. 43.73 ± 0.5474 g in db/db; $p < 0.0001$; $n = 8$) and glycemia (138.5 ± 3.674 mg/dl in db/+ vs. 563.0 ± 19.80 mg/dl in db/db; $p < 0.0001$; $n = 8$). These data confirmed that db/db mice used during this study were diabetic.

2.4. Immunohistochemistry

Human and mouse eyes embedded in paraffin were sectioned (3 μm) along the eye axis, deparaffinized and rehydrated. For antigen retrieval, a solution of citrate was used to unmask the epitopes of the retinal sections. After several washes in phosphate buffered saline (PBS), retinal sections were incubated overnight at 4 °C with the following primary antibodies: rabbit anti-endostatin (Invitrogen, Carlsbad, CA, USA, PA1-601) at 1:100 dilution, obtained by immunizing a rabbit with two peptides corresponding to amino acids 129–142 from mouse and human endostatin; goat anti-mouse collagen IV (Merck Millipore, Billerica, MA, USA) at 1:20 dilution; mouse anti-mouse PKCα (Sigma-Aldrich, St Louis, MO, USA) at 1:100 dilution; goat anti-mouse cone arrestin (Santa Cruz Biotechnology, Heidelberg, Germany) at 1:100 dilution; rabbit anti-mouse GFAP (DAKO, Glostrup, Denmark) at 1:1000 dilution; rabbit anti-mouse MMP-2 (Abcam, Cambridge, UK) at 1:500 dilution; rabbit

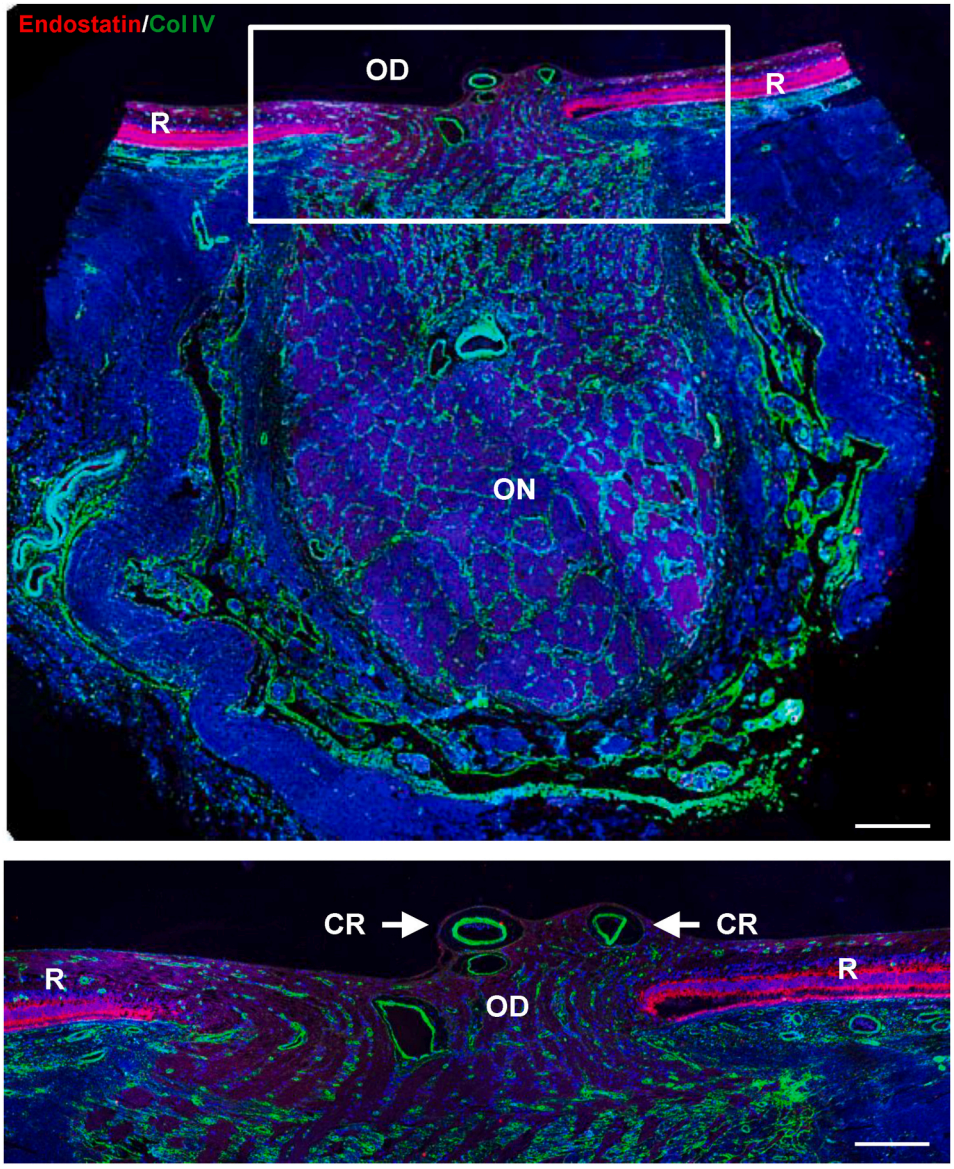

Fig. 6. Human optic disc was practically devoid of endostatin. Double immunostainig with anti-endostatin and anti-collagen IV antibodies showed a markedly endostatin accumulation in the neuroretina, whereas as happens in mouse retina, endostatin was unobservable in the optic disc. The figure is a mosaic composite obtained from different captures at 63X in the laser scanning confocal microscope. OD: Optic disc; ON: Optic nerve; CR: Central retinal artery and vein; R: Retina. Scale bar: 474.92 μm; 226.15 μm (inset).

anti-mouse MMP-9 (Proteintech, Rosemont, IL, USA) at 1:100 dilution. All primary antibody solutions were diluted with donkey serum (Sigma-Aldrich) at 1:10 dilution as a blocking agent to prevent secondary antibody unspecific binding. After washing the sections in PBS, they were incubated 2 h at room temperature with specific fluorochrome-conjugated secondary antibodies diluted at 1:100: donkey anti-goat Alexa 488 (Life Technology, Carlsbad, Ca, USA); goat anti-rabbit 488, rabbit anti-goat Alexa 568, and goat anti-rabbit 568 (Invitrogen). Hoechst (Sigma-Aldrich) diluted in PBS (1:100 dilution) was used for nuclear counterstaining. Slides were mounted in Fluoromount (Sigma-Aldrich) medium for further analysis using a laser scanning confocal microscope (TCS SP2 or TCS SP5; Leica Microsystems GmbH, Heidelberg, Germany). Immunohistochemistry negative control was done by omission of the primary antibody in a sequential tissue section. To verify anti-endostatin antibody specificity, blocking peptide assay, FcR blocking, and isotype control assay were performed on eye paraffined sections. For blocking peptide assay, the neutralization of the primary anti-endostatin antibody was done in a previous incubation step of 1 h before immunohistochemistry by adding 10-times excess of recombinant mouse endostatin (R&D Systems, MN, Minneapolis), in contrast to the control incubated with the anti-endostatin antibody alone. For FcR blocking, paraffin sections were incubated with Mouse Seroblock FcR (Bio-Rad Laboratories, Hercules, CA, USA) at 1:100 dilution during 1 h before the start of the immunohistochemistry process in order to prevent non-specific binding of the Fc fragment from the Endostatin's IgG to the mouse Fc receptors FcRγIII and FcR&gamma:II. For isotype control assay, we used an antibody matching the host and IgG isotype of anti-endostatin antibody that targets an antigen absent in the retina. Anti-endostatin antibody's host is rabbit, which has only one subclass of IgG isotype (Weber et al., 2017). Thus, we used a rabbit antibody against collagen I (abcam), which is highly expressed in cornea and absent in the retina (Ruberte et al., 2017).To assess retinal morphology and location of intravitreal vessels, eye paraffin sections were stained with Hematoxylin/Eosin and were observed with a light microscope (Nikon Eclipse E800).

2.5. Western blot analysis

For protein extraction, mouse eyes were enucleated and each retina was immediately dissected in PBS and homogenized in RIPA lysis buffer (25 mM Tris base, pH 8.2, 150 mM NaCl, 0.5% NP-40, 0.1% SDS, 0.5% sodium deoxycholate), containing protease inhibitor cocktail tablets

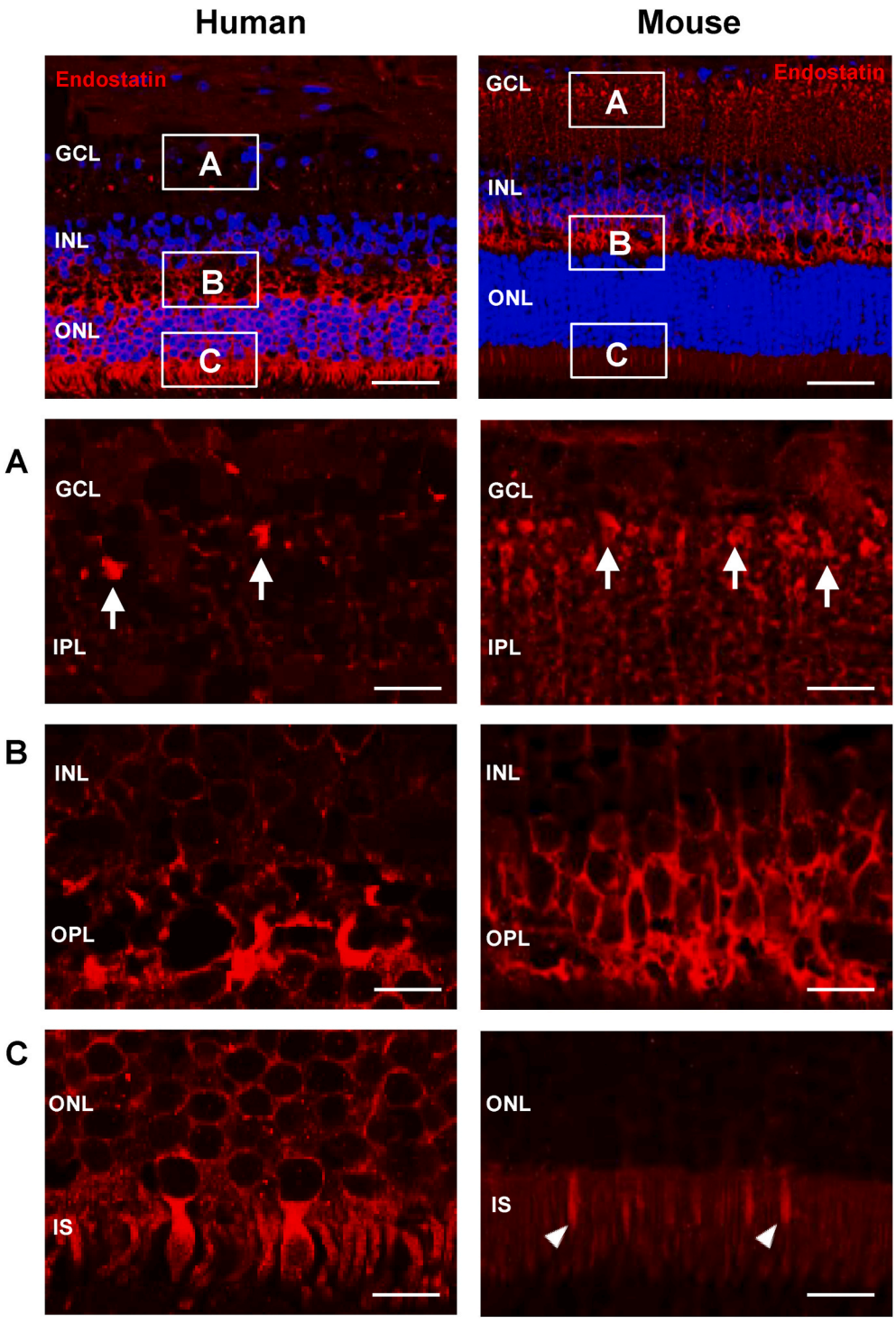

Fig. 7. Comparison between human and mouse endostatin distribution in neuroretina. Immunolabelling with anti-endostatin antibody in human and mouse retinas showed a similar, although with some differences, endostatin distribution in both species, mainly located at bipolar cells and photoreceptors. (**A**) Human bipolar terminal axons (arrows) showed lower expression of endostatin compared to mouse retina. (**B**) Bipolar cell perikaryal were stained with endostatin in both human and mice retina with a similar intensity. (**C**) In contrast with mice, where only scarce cones (arrowheads) showed endostatin accumulation in their inner segments, human retina showed a higher signal of endostatin at photoreceptors, suggesting that both cone and photoreceptors accumulated endostatin. The same anti-endostatin antibody was used on both human and mice retinal sections. GCL: ganglion cell layer; IPL: inner plexiform layer; INL, inner nuclear layer; OPL: outer plexiform layer; ONL: outer nuclear layer; IS: inner segments of photoreceptors. Scale bars: 38.3 μm; 10.64 μm (A, B, C).

(Complete Mini, Roche, Basel, Switzerland). After vortex, retinas were centrifuged at 8000 g for 10 min. BCA assay reagent (Sigma-Aldrich) was used for each sample to determine total protein concentration.

For immunoblotting, 50 mg of protein of each sample were individually resuspended in 50% sample loading buffer (140 mM Tris base, pH 6.7, 6.8% SDS, 33% glycerol, 0.004% bromophenol) and 5% β-mercaptoethanol (Sigma-Aldrich) and heated at 95 °C for 5 min. Afterwards, 12 μl of each sample were loaded in a 12% pre-cast SDS-PAGE gel (Bio-Rad) for electrophoresis followed by protein transfer to a polyvinylidene difluoride (PVDF) membrane (Merck Millipore). PVDF membranes were blocked with 2% BSA in TBST (Tris buffered saline, 0.05% Twen 20) for 1 h at room temperature and incubated with rabbit anti-mouse endostatin antibody (Invitrogen) at 1:100 dilution overnight at 4 °C. After washing in TBST, the membrane was incubated with secondary antibody horseradish peroxidase-conjugated goat anti-rabbit (Bionova Scientific, Fremont, CA, USA) at 1 : 5000 dilution for 45 min at room temperature. Both primary and secondary antibodies were also diluted with 2% BSA in a 0.05% TBST.

Following antibodies incubation, the reagent Luminata Crescendo (Merck Millipore) was used for chemiluminescent detection. The bands revealed with Fluor-S Max imager (Bio-Rad) were analyzed with Image J software (National Institutes of Health, Bethesda, MD, USA) and rabbit

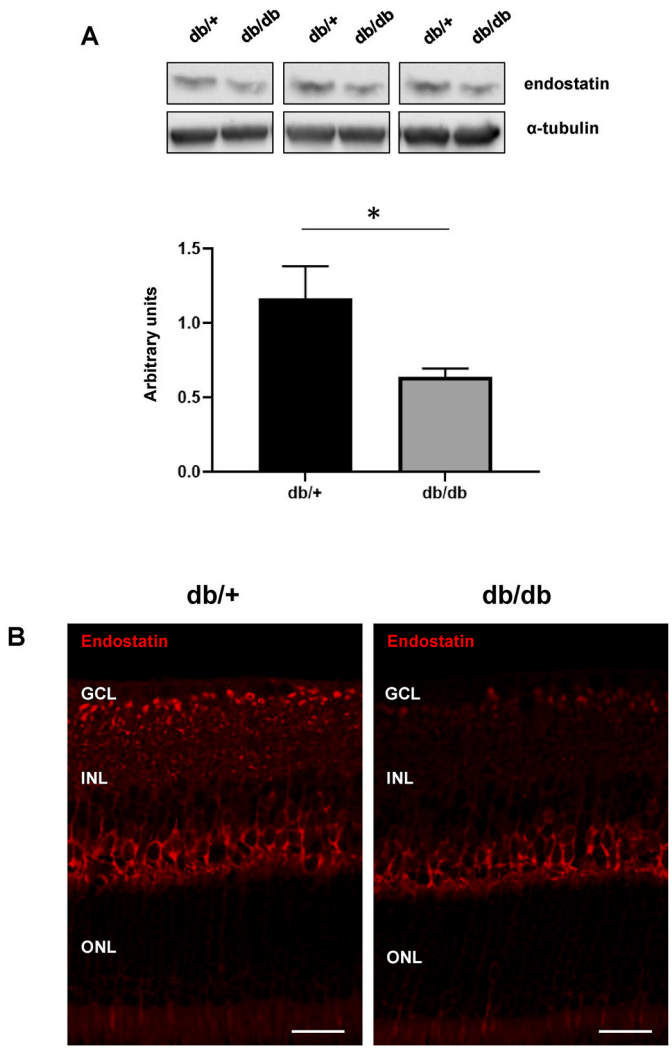

Fig. 8. Endostatin is decreased in db/db mouse retinas. (**A**) Western blot analysis revealed that endostatin protein expression was 0.5-fold decreased in 12 weeks-old diabetic mouse retinas, especially in the ganglion cell layer. Statistical analysis showed significant differences in endostatin band intensity between db/+ and db/db mice (1.275 ± 0.126 arbitrary units in db/+ mice vs. 0.753 ± 0.055 arbitrary units in db/db mice; $p = 0.019$; n = 3). α-tubulin was used as a loading control (**B**) Immunofluorescence representative images showing decreased endostatin expression in db/db retinas. Nuclei were counterstained with Hoechst. OD: Optic disc; CR: Central retinal vessel; R: Retina. Scale bar: 22.22 μm.

anti-mouse α-tubulin (Abcam) at 1:500000 dilution was used as a loading control to normalize the levels of the protein of interest. Recombinant mouse endostatin was also run in the same gel to compare the molecular wheight of retinal endostatin and the isolated peptid. A total of 3 repetitions were performed in each Western blot.

2.6. Scanning laser ophthalmoscopy (SLO)

Mice were anaesthetized using a ketamine (12 mg/kg) and xylazine (100 mg/kg) cocktail diluted in physiological saline solution and injected intraperitoneally. Toe pinch was performed to assure a correct anesthetic status and respiratory function was monitored during the process. Once mice were anaesthetized, eye drops of anesthetic collyrium and tropicamide (Alcon, Barcelona, Spain) were administered to induce mydriasis. To prevent the eye from drying and developing cataracts, Viscofresh (Allergan, Dublin, Ireland) was continuously applied on both eyes and custom-made mouse lenses were placed on the corneas to visualize retinal blood vessels. 10 μl of 5% sodium fluorescein (Sigma-Aldrich) were injected subcutaneously in each mouse and angiography was performed with HRA2 Imaging Instrument (Heidelberg Engineering, Heidelberg, Germany). Angiography was performed in every mouse retina in both eyes and all vascular plexi were analized, paying especial attention to the vessels that protruded into the vitreous from the optic disc.

2.7. Vessel density quantification

Vascular density of the entire retina and the central area was quantified using Angiotool software (Zudaire et al., 2011) in both groups. The results were represented in % of vessels area.

2.8. Statistical analyses

Statistical analyses were performed using R Statistical Software (version 4.1.0; R Foundation for Statistical Computing, Vienna, Austria). Shapiro-Wilk test and F test were performed for the evaluation of data distribution and variance homogeneity, respectively. For normal distribution and homogenous variances, the parametric method unpaired *t*-test was used. For data not normally distributed the Wilcoxon test was performed. Data are expressed as mean ± standard error of the mean (SEM). Difference between groups was considered significant at P-value<0.05.

3. Results

3.1. Endostatin is expressed in mouse and human retinal neurons

Cross-reactivity of anti-endostatin antibodies with collagen XVIII, the endostatin precursor, is one of the challenges to immunolocalize cleaved active endostatin, since antibodies used to date in retinal studies also recognize uncleaved endostatin and mark almost exclusively blood basement membranes and the internal limiting membrane (Pehrsson et al., 2019). To try to solve this situation we used a polyclonal anti-endostatin antibody which previously had demonstrated its ability to detect endostatin intracellularly (Martín-Granado et al., 2017; Huaman et al., 2019). To confirm antibody specificity for cleaved endostatin, several assays were performed in retinal sections. First, a blocking peptide assay was used to neutralize the primary anti-endostatin antibody with recombinant mouse endostatin (Fig. 1A). In addition to this, blocking Fc assay (Fig. 1B) that specifically blocks mouse Fc receptors in the retina, and isotype control assay (Fig. 1C) that guarantees non-specific binding of similar IgG isotypes, were performed. Furthermore, Western blot analyses showed that bands of retinal endostatin and recombinant endostatin were comparable and around 20 kDa (Fig. 2), the stablished molecular weight of cleaved endostatin (Marneros et al., 2004; Cristante et al., 2018). Lane 1 shows a different number of bands compared to lane 2 (Fig. 2), probably due to the fact that lane 1 corresponds to native endostatin from the retinal tissue and lane 2 corresponds to recombinant endostatin. Recombinant endostatin is a purified peptide that might have not suffered the same post-translational modifications. In addition to this, mouse endostatin peptides can have deletions or extensions of few residues at the N or C-terminal (Yamaguchi et al., 1999) that could explain why native endostatin shows more bands and a slightly different weigh compared to the recombinant endostatin.

In mouse retinas, endostatin distribution was similar throughout the central and peripheral retina, but at the level of the optic disc endostatin was unobservable (Fig. 3A). Endostatin signal was found inside retinal neurons, without marking neither the internal limiting membrane nor the blood vessel basement membranes (Fig. 3B), which confirmed that the antibody was only detecting cleaved endostatin and not collagen XVIII.

Given that the distribution of the endostatin signal was compatible with the morphology of bipolar cells (Fig. 4), dual immunostaining with

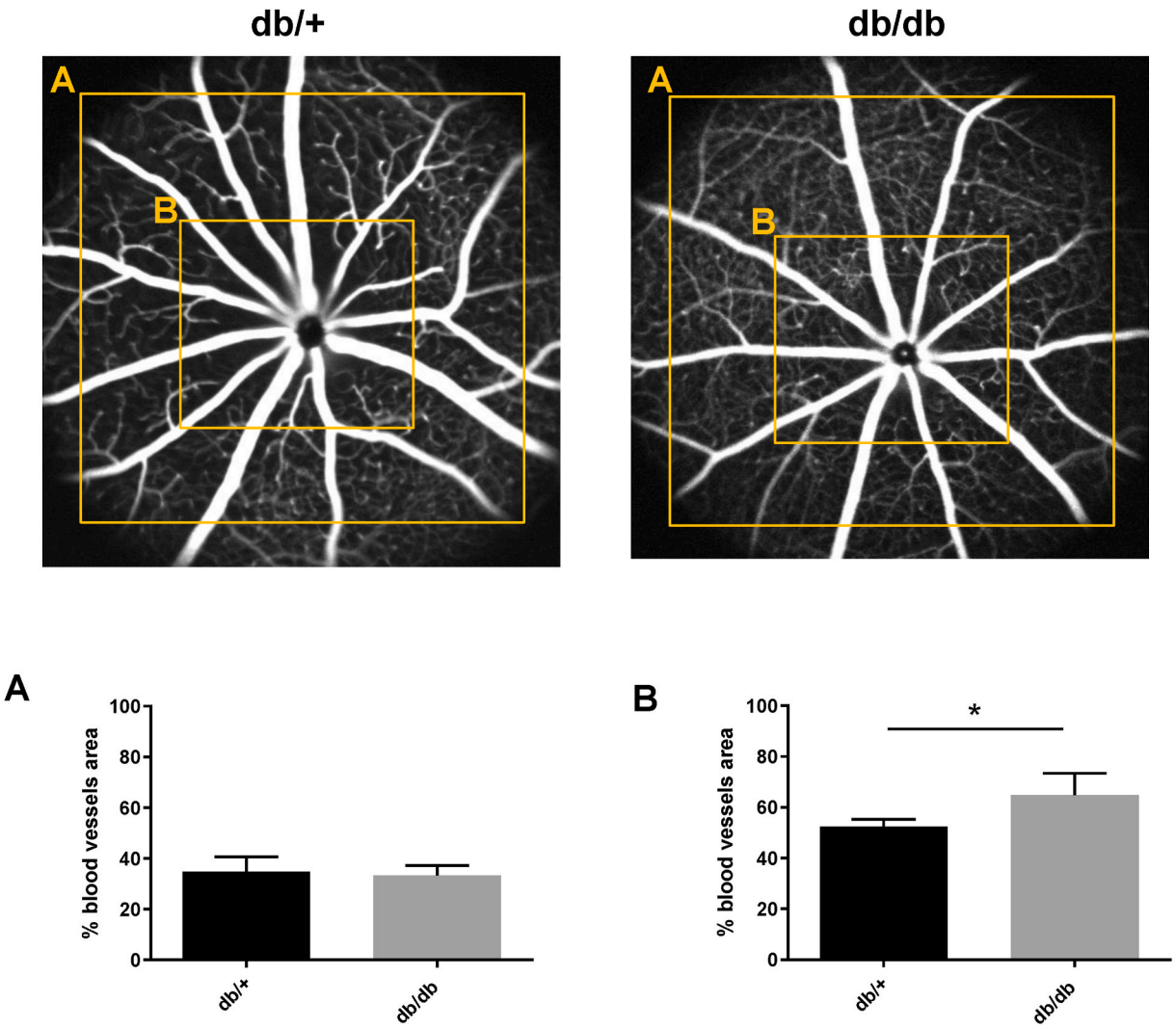

Fig. 9. Vascular density in central retina was increased in db/db mice. *In vivo* fundus fluorescein angiography was performed to assess retinal vascularization. (**A**) No significant differences in vascular density were found when comparing the entire retinal vascular network (34.82 ± 2.32% vessel area in db/+ retinas vs. 33.35 ± 1.56% vessel area in db/db retinas; $p = 0.652$; n = 5) in 12 weeks-old mice. (**B**) However, a statistically significant increase in vascular density was found in the central part of the retina of db/db mice (52.47 ± 1.12% vessel area in db/+ retinas vs. 64.87 ± 13.39% vessel area in db/db retinas; $p = 0.046$; n = 5) in 12 weeks-old mice.

anti-PKCα antibody, a specific marker of rod bipolar cells (Haverkamp et al., 2003), was performed. The result showed that endostatin was accumulated in bipolar cell axon terminals but not in the axons themselves (Fig. 4A). Dendrites, including their terminals, and the perikaryon of bipolar cells also accumulated endostatin (Fig. 4B). Although endostatin was mainly located at the internal neuroretina, sporadic photoreceptors also showed intracellular endostatin (Fig. 5). To identify what type of photoreceptor accumulates endostatin, cone arrestin, a specific marker of cone photoreceptors (Zhu et al., 2002), was employed. Dual immunostaining with anti-cone arrestin antibody showed that endostatin was accumulated in the inner segments of cone photoreceptors. The cone synaptic terminals did not accumulate endostatin (Fig. 5).

Interestingly, the distribution pattern of endostatin in human retina was similar to the mouse retina. Endostatin was also undetectable in the human optic disc (Fig. 6) and was also accumulated in bipolar cells and photoreceptors (Fig. 7). However, some minor differences were found, namely a lower accumulation of endostatin in the bipolar cell axons terminals (Fig. 7A), although bipolar perikaryal were stained with similar intensity (Fig. 7B), and a higher number of photoreceptors with intracellular endostatin (Fig. 7C). The morphology of these photoreceptors suggested that both cone and rods accumulated endostatin in the human retina (Fig. 7C).

3.2. Endostatin is decreased in db/db mouse retinas

Once established the presence of endostatin in mouse and human retinal neurons and given that eye concentrations of endostatin in patients with diabetic retinopathy significantly correlates with the severity of the disease (Funatsu et al., 2003), we next investigated the concentration of endostatin in the retina during experimental hyperglycemic conditions. Western blot analysis of db/db mice, a well stablished model of type 2 diabetes (Robinson et al., 2012; Bogdanov et al., 2014), showed a statistically significant decrease (0.5-fold change) of endostatin in the neuroretina of diabetic mice (1.275 ± 0.126 arbitrary units in db/+ mice vs. 0.753 ± 0.055 arbitrary units in db/db mice; $p = 0.019$; n = 3) (Fig. 8A). In addition, in some db/db mice endostatin decrease was exacerbated in ganglion cell layer (Fig. 8B).

3.3. Optic disc intravitreal vascularization in db/db mouse retinas

Given that endostatin is an inhibitor of angiogenesis preventing endothelial cell proliferation, migration, and invasion (Kim et al., 2002),

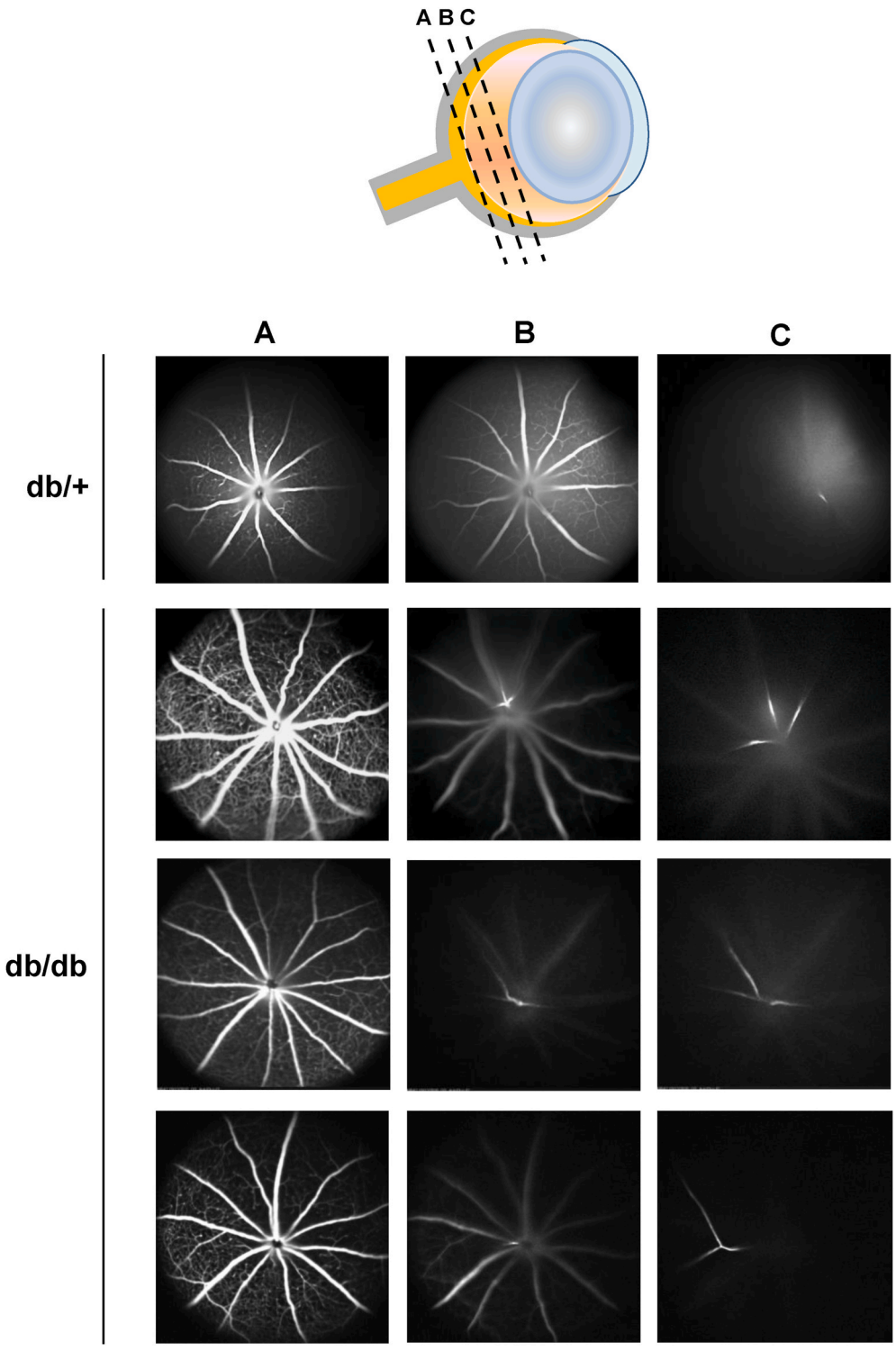

Fig. 10. Intravitreal vessel angiography in db/db mouse retinas. After fluorescein injection, three consecutives focal planes of the eye fundus (A, B, and C) were performed to assess intravitreal vessels. 50% of db/db mice presented intravitreal vessels while only one db/+ presented a single tiny intravitreal vessel (n = 8). In the most part of db/db mice several vessels, usually three, invaded the vitreous from the optic disc.

we next analyzed whether the decrease of endostatin in the retina of diabetic mice led to neovascularization. Retinal blood vessels were investigated using *in vivo* eye fundus fluorescein angiography (Fig. 9) and the AngioTool software (Zudaire et al., 2011) was used to quantify vascular density. The results showed not significant differences in vascular density between 12-week-old db/db and db/+ mice, when the entire retinal vascular network was compared (34.82 ± 2.32% vessel area in db/+ retinas vs. 33.35 ± 1.56% vessel area in db/db retinas; $p = 0.652$; n = 5) (Fig. 9A). This agrees with most of the data provided by the bibliography, which indicate that neovascularization is not a frequent finding in db/db mouse retina (Li et al., 2010; Bogdanov et al., 2014; Kim et al., 2014). To our knowledge, neovascularization in db/db mice retina has only been reported in a single study using long-standing 15-month-old mice (Cheung et al., 2005). However, when the vascular

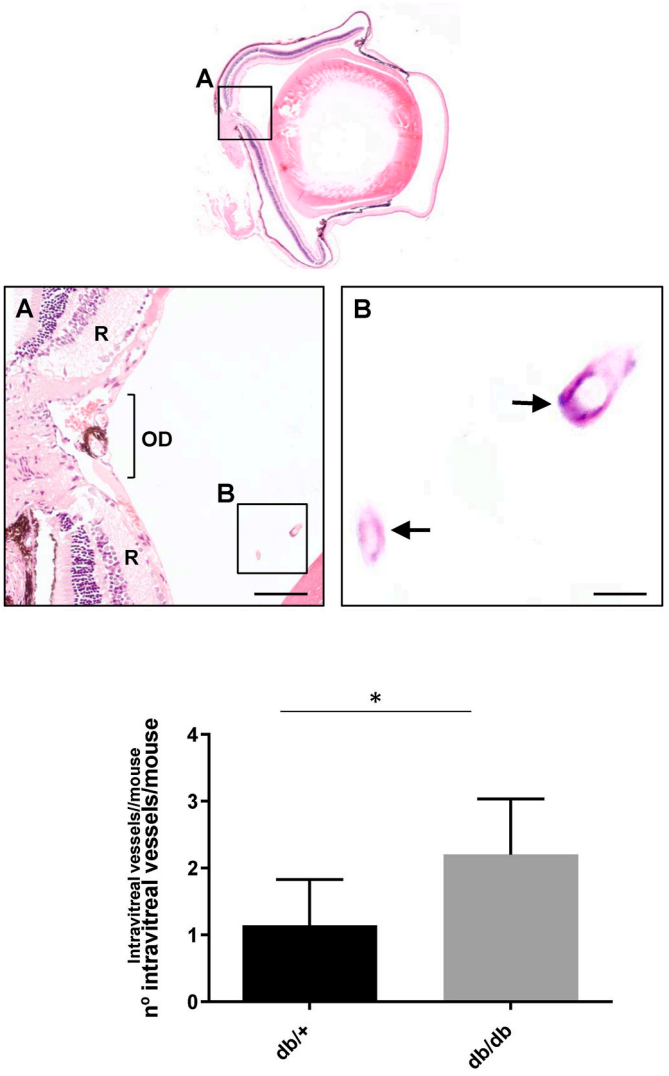

Fig. 11. Intravitreal vessel histology in db/db mouse retinas. Paraffin sections of the retina sectioned along the eye axis were counterstained with Hematoxylin/Eosin. A significant increase of intravitreal vessels (arrows) in db/db mice was observed (1.143 ± 0.261 number of intravitreal vessels in db/+ mice (n = 7) vs. 2.200 ± 0.374 number of intravitreal vessel in db/db mice (n = 5); p = 0.037). OD: Optic disc; R: Retina. Scale bar: 76.45 μm (A); 12.23 μm (B).

density was compared in the central part of the retina, a significant slight vascular density increase was observed in diabetic mice (52.47 ± 1.12% vessel area in db/+ retinas vs. 64.87 ± 13.39% vessel area in db/db retinas; p = 0.046; n = 5) (Fig. 9B).

To confirm whether this increased vascular density in the central part of the retina was compatible with optic disc vessels protruding into the vitreous, we acquired three different focal planes of the eye fundus using SLO (Fig. 10 A, B, C). Using this approach, optic disc vessels protruding the vitreous can be easily identified (Fig. 10). The results obtained showed that 50% of the db/db mice (n = 8) presented vessels that originated from the optic disc and invaded the vitreous. Furthermore, in comparison with db/+ mice, where only one animal presented a single small vessel contacting the vitreous, in most db/db mice several vessels, usually three, invaded the vitreous (Fig. 10). This result correlated with histological analysis in paraffin eyes sections studied at the level of the optic disc, where the number of recognizable intravitreal blood vessels identified by Hematoxylin/Eosin staining was significantly increased in db/db mice (1.143 ± 0.261 number of intravitreal vessels in db/+ mice (n = 7) vs. 2.200 ± 0.374 number of intravitreal vessel in db/db mice (n = 5); p = 0.037) (Fig. 11).

3.4. Optic disc intravitreal vessel phenotype in db/db mice

Once established that 50% of 12-week-old db/db mice studied had vessels that from the optic disc penetrated the vitreous, we tried to answer the question about the nature of these vessels. Basically, two possibilities existed: (a) they were persistent hyaloid vessels or (b) they were neovessels triggered by the pro-angiogenic environment induced by the decrease of endostatin in the db/db mouse retina.

During development, the intraocular structures are nourished by the hyaloid vascular system (Saint-Geneiz and D'Amore, 2004). This vascular system in mouse starts to form at embryonic day 10.5 and becomes fully developed by embryonic day 13.5 (Smith et al., 2002). It is widely accepted that the hyaloid vascular system in mice initiates its regression after birth and totally disappears around postnatal days 14–24 (Ito et al., 1999; Fukai et al., 2002; Ohlmann et al., 2004; Ritter et al., 2005). In a previous study from our group, 15% of 25-week-old wild type C57BL/6J mice showed functional persistent hyaloid vessels (McLenachan et al., 2015), which matches with the presence of a small intravitreal vessel found in one db/+ mice (representing the 16% of the db/+ analyzed). However, 50% of db/db retinas presented intravitreal vessels, which largely exceeded the normal percentage of expected persistent hyaloid vessels in a non-diabetic mouse. In this regard, mice lacking collagen XVIII/endostatin showed ocular abnormalities including a delay in normal postnatal regression of hyaloid vessels (Fukai et al., 2002). Similarly, hyaloid vessels also persisted in collagen XVIII human mutations (Knobloch syndrome) (Sertié et al., 2000).

Although these arguments could suggest that intravitreal vessels found in db/db mouse retinas were persistent hyaloid vessels, delayed regression of hyaloid vessels in collagen XVIIII/endostatin null mice leads to abnormal disorganized vascularization of the entire retina (Fukai et al., 2002), situation that we never found in db/db mouse retinas (Fig. 8). Furthermore, the morphological aspect of intravitreal vessels in db/db mice was similar to human papillovitreal neovessels during diabetic retinopathy (L'Esperance, 1998). Thus, to discriminate whether intravitreal vessels found in db/db mice were persistent hyaloid vessels or neovessels, we analyzed them by immunofluorescence in 8-week-old db/db mice. Intravitreal db/db vessels showed an incomplete lining of GFAP positive signal (Fig. 12), what would indicate that db/db intravitreal vessels were partially surrounded by neuroglial cells. Similarly, it is well stated that preretinal neovessels expressed GFAP in their walls during proliferative diabetic human retinopathy (Smith et al., 1999). In contrast, published data about the presence of neuroglia surrounding persistent hyaloid vessels is contradictory. In Nuc1 spontaneous rat and in humans with persistent fetal vasculature (PFV) it has been described that astrocytes sheath the persistent hyaloid artery (Zhang et al., 2005). This abnormal association of astrocytes with the hyaloid artery may impede the normal macrophage-mediated remodelling and regression of the hyaloid system (Zhang et al., 2011). However, in collagen XVIII/endostatin null mice persistent hyaloid vessels are devoid of neuroglial coverage (Hurskainen et al., 2005).

Intravitreal db/db vessels showed a thickening of their basement membrane due to increased collagen IV deposition (Fig. 13A), which is the main component of the retinal vessel basement membrane (Inoue, 1989), compared to the intraretinal vessels (Fig, 13B). Basement membrane thickening and increased collagen IV deposition are hallmarks of diabetic retinopathy (Roy et al., 2010). However, this is not a differential clue used to distinguish between persistent hyaloid vessels and intravitreal neovessels, because degenerating hyaloid vessels (Kishimoto et al., 2018) and persistent hyaloid vessels (Hurskainen et al., 2005) present also increased collagen IV deposition in their thicker basement membranes.

Degradation of extracellular matrix components is thought to be essential for the development of neovessels in proliferative diabetic retinopathy. Several species of MMPs are capable of degrading various extracellular matrix molecules and have been detected in the fibrovascular tissues in eyes with diabetic retinopathy (Roy et al., 2010).

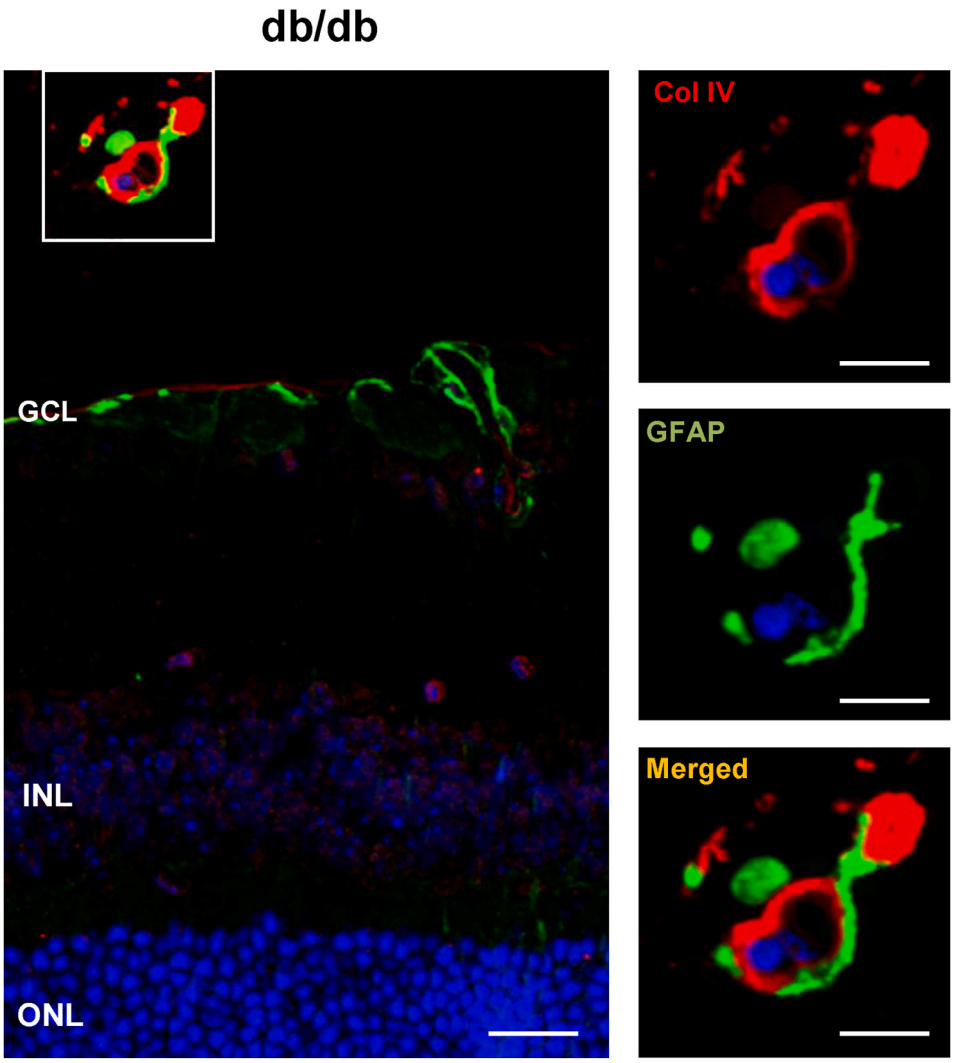

Fig. 12. GFAP expression surrounding intravitreal vessels in db/db retinas. Double immunofluorescence using collagen IV and GFAP showed that intravitreal vessels in 8 weeks db/db mice were covered partially by neuroglia. Nuclei were counterstained with Hoechst. GCL: ganglion cell layer; INL: inner nuclear layer; ONL: outer nuclear layer. Scale bar: 23.82 μm; 12.54 μm (inset).

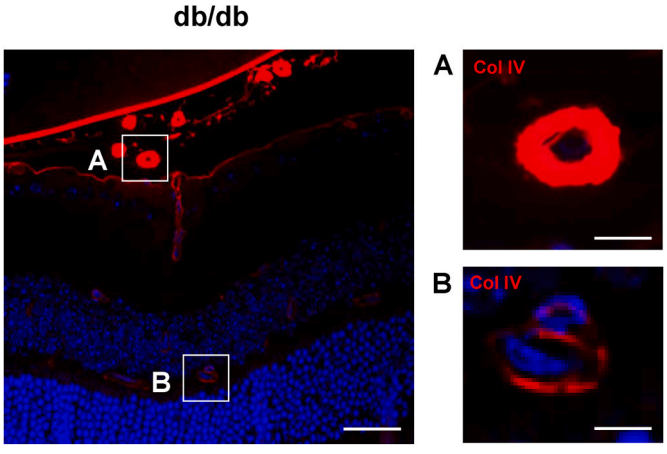

Fig. 13. Thickening of intravitreal vessel basement membrane in db/db mice. Immunodetection of collagen IV in 8 weeks-old db/db mice retinas showed a thickening in the basement membrane of intravitreal vessels (A) compared to the intraretinal vessels (B). Nuclei were counterstained with Hoechst. GCL: ganglion cell layer; INL: inner nuclear layer; ONL: outer nuclear layer. Scale bar: 35.74 μm; 8.69 μm (A); 7,35 μm (B).

Specifically, MMP-2 and -9 have been immunohistochemically detected in the wall of intravitreal human neovessels (Noda et al., 2003). In the same way, intravitreal db/db vessels showed MMP-2 (Fig. 14) and MMP-9 (Fig. 15) co-localizing with collagen IV, a substrate of these MMPs (Somerville et al., 2003). Although finding both basement membrane thickening and degradation by MMPs in intravitreal db/db vessels may seem counterintuitive, it may be explained as a compensatory response to increased synthesis of basement membrane components during diabetic retinopathy (Roy et al., 2010).

4. Discussion

Endostatin, the carboxyl-terminal fragment of type XVIII collagen, is a natural inhibitor of angiogenesis and its effect is being tested and proven effective in several clinical eye studies. RetinoStat, an equine infectious anemia virus-based lentiviral gene therapy vector that expresses endostatin and angiostatin, has been demonstrated to have activity against choroidal neovascularization and it was well tolerated and capable of persistent expression after subretinal delivery (Kachi et al., 2009). Furthermore, Tat PTD-Endostatin-RGD, a novel fusion protein, inhibited abnormal angiogenesis in retina via eye drops (Li et al., 2016). However, despite its therapeutic use, comprehensive research about the role of endostatin during diabetic retinopathy is scarce (Noma et al.,

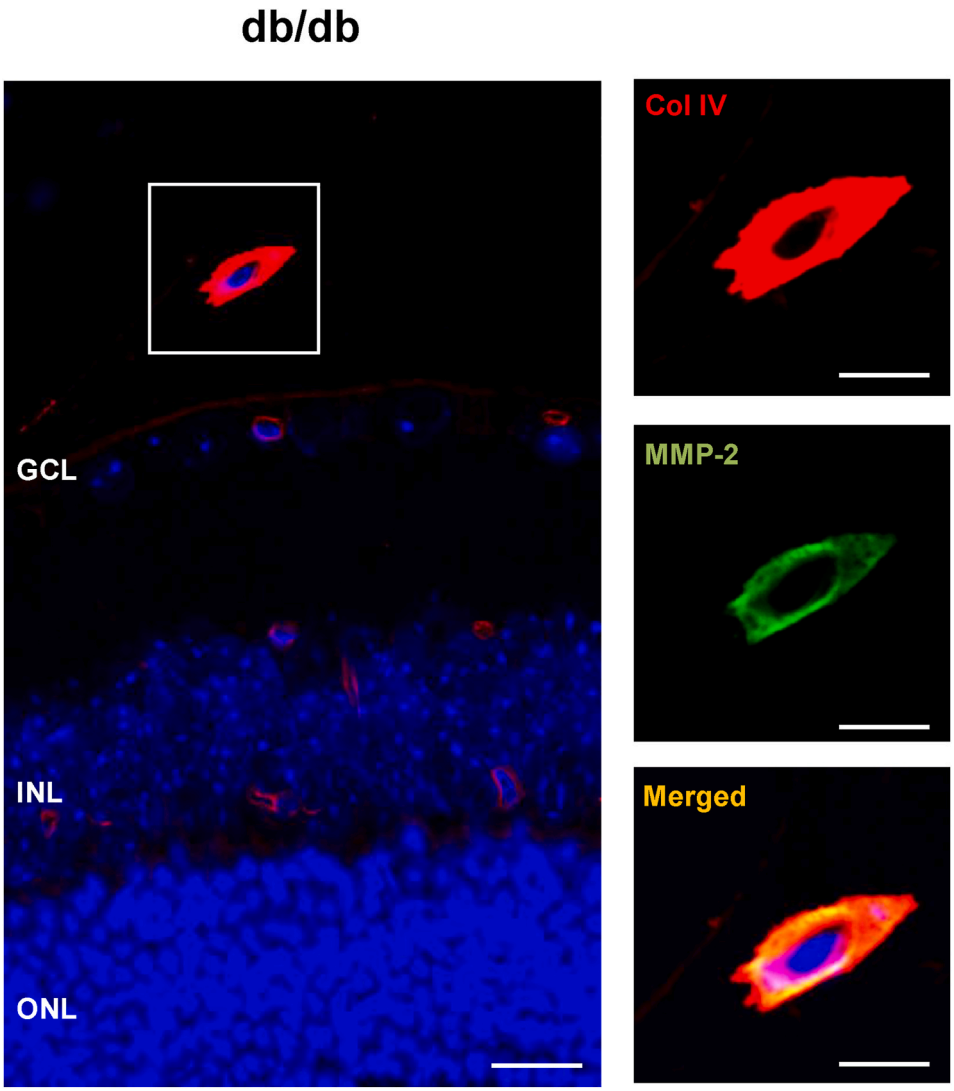

Fig. 14. MMP-2 expression in the basement membrane of intravitreal vessels of db/db mice. Immunofluorescence analysis showed that collagen IV and MMP-2 co-localized in the basement membrane of 8-week-old db/db mice intravitreal vessels. Nuclei were counterstained with Hoechst. GCL: ganglion cell layer; INL: inner nuclear layer; ONL: outer nuclear layer. Scale bar: 18.49 μm; 9.24 μm (inset).

2002; Funatsu et al., 2003).

This study revealed for the first time the presence of intracellular endostatin in mouse and human retinal neurons. The observations made showed that endostatin was accumulated in the dendrites and axons of bipolar cells and in photoreceptors, mainly in their inner segments. The question about whether endostatin has intracellular or extracellular location is an important variable when considering likelihood of substrate/enzyme interaction. To date, endostatin in neuroretina has been only found extracellularly in basement membranes (Takahashi et al., 2003; Bhutto et al., 2004; Ohlmann et al., 2004; Ramesh et al., 2004; May et al., 2006; Määttä et al., 2007), where collagen XVIII may be cleaved by MMPs, elastases, and other extracellular proteases (Ferreras et al., 2000). However, similarly as what occurs in our study, healthy neurons containing intracellular endostatin have been found in the human cortex (Deininger et al., 2002). An explanation for this intracytoplasmic localization of endostatin could be cathepsin B, a lysosomal protease, which can generate endostatin from collagen XVIII (Im et al., 2005). Cathepsin B has been found to colocalize intracellularly with endostatin in neurons. Although intracellular localization of endostatin has been correlated with cell apoptosis (Hou et al., 2010), other studies in isolated retinal astrocytes suggested that intracellular endostatin is secreted extracellularly by exosomes (Hajrasouliha et al., 2013). Exosomes are nanometer-sized vesicles that cells can release in a controlled manner to mediate a plethora of cellular activities, including neovascularization (Klingeborn et al., 2017). Very little research on the role of exosomes in diabetic proliferative retinopathy has been done to date, although it is known that exosomes containing endostatin suppress choroidal neovascularization (Hajrasouliha et al., 2013). Investigating the role of endostatin containing exosomes from retinal neurons may identify antiangiogenic based mechanisms, which could help to develop novel therapeutic targets to control aberrant retinal neovascularization.

Diabetic db/db mice showed a reduction of endostatin in their retinas. Furthermore, in some db/db mice endostatin was especially decreased in the ganglion cell layer. However, this result is not conclusive and further studies will be necessary to clarify to what extend endostatin decrease is different among retinal layers in db/db mice. Endostatin reduction was associated with the appearance of vessels that originated from the optic disc and penetrated to the adjacent vitreous in the 50% of db/db mice. Whether these intravitreal vessels found in db/db mice were persistent hyaloid vessels at 84 postnatal day (12-week-old), when in fact they should have disappeared completely at 14–24 postnatal days (Ito et al., 1999; Fukai et al., 2002; Ohlmann et al., 2004; Ritter et al., 2005), or neovessels induced by the pro-angiogenic environment developed by the decrease of endostatin, is a question that our

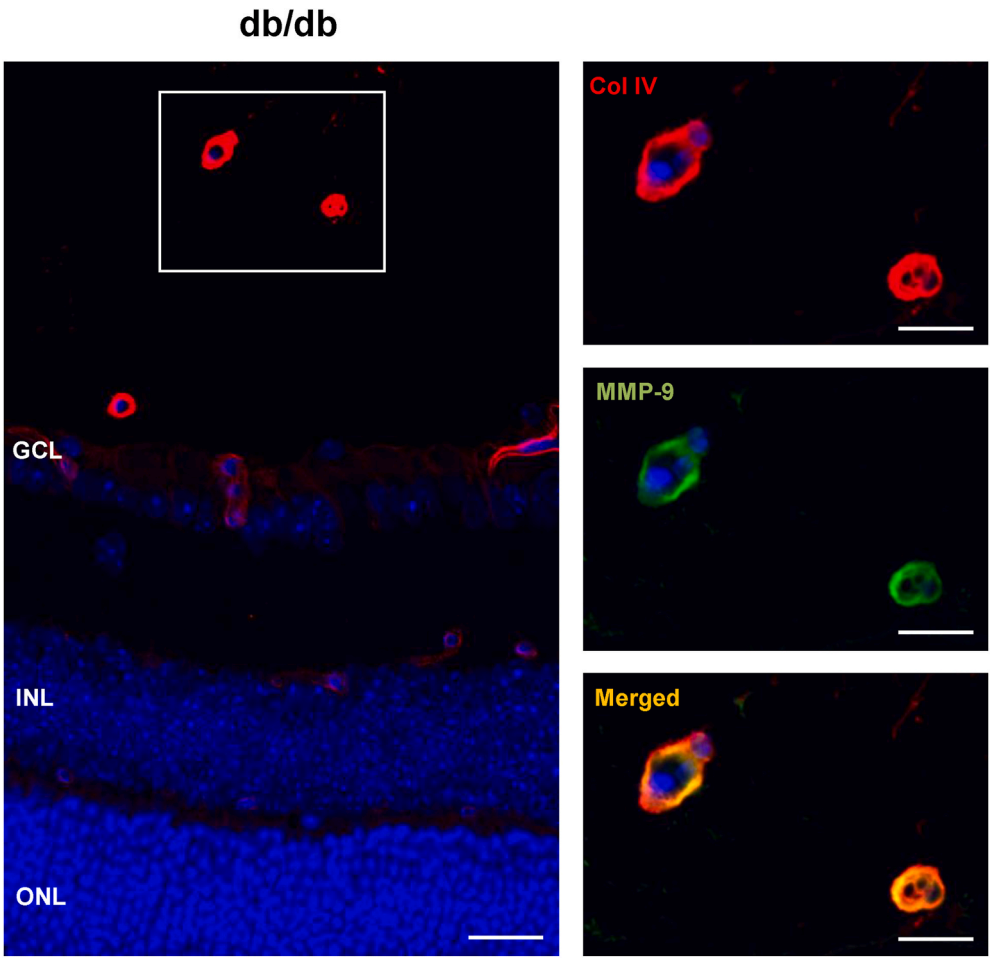

Fig. 15. MMP-9 expression in the basement membrane of intravitreal vessels of db/db mice. Immunofluorescence analysis showed that collagen IV and MMP-9 co-localized in the basement membrane of 8-week-old db/db mice intravitreal vessels. Nuclei were counterstained with Hoechst. GCL: ganglion cell layer; INL: inner nuclear layer; ONL: outer nuclear layer. Scale bar: 17.82 μm 8.91 μm (inset).

study has not been fully able to answer.

The intravitreal vessel phenotype in db/db mice revealed features such as GFAP positive sheath of neuroglia and a thicker basement membrane, which are hallmarks of neovessels in diabetic retinopathy (Smith et al., 1999; Roy et al., 2010). However, they also appear in persistent hyaloid vessels (Hurskainen et al., 2005; Zhang et al., 2005). In contrast, the presence of MMP-2 and MMP-9 at the basement membrane in db/db intravitreal vessels, which is characteristic of human diabetic neovessels (Noda et al., 2003), has not been described, to our knowledge, in persistent hyaloid vessels. Since endostatin inhibits MMP-2 (Kim et al., 2000), its decrease in db/db mice retinas could explain the presence of metalloproteinase in the wall of intravitreal vessels. All together, these findings could suggest that neovascularization may occur at the optic disc in hyperglycemic db/db mice. However, it cannot be ruled out that these intravitreal vessels may also represent non-degenerated hyaloid vessels.

Finally, the human optic disc represents a preeminent site for the appearance of neovessels during proliferative diabetic retinopathy. Two situations occur during diabetic neovascularization: appearance of new blood vessels on the optic disc (NVD), which frequently lead to visual loss, and appearance of new blood vessels elsewhere on the retina (NVE), which do not pose such a serious threat to vision (Valsania et al., 1993). The almost null presence of anti-angiogenic endostatin in the human optic disc, could explain why the optic disc is prone to neovascularization during human diabetic retinopathy.

5. Conclusions

For the first time, this study revealed the presence of endostatin in bipolar cells and photoreceptors, in both mouse and human retinas. Endostatin expression was inappreciable at the level of the optic disc, which could explain why this location is susceptible to neovascularization in diabetic retinopathy. Furthermore, endostatin was decreased in diabetic mouse retina. Diabetic db/db mice also presented significantly increased number of intravitreal vessels protruding from the optic disc. These intravitreal vessels showed a GFAP positive neuroglia sheath, basement membrane thickening, and expressed metalloproteinases in the vascular wall, suggesting that they could be neovessels similar to the papillovitreal neovessels observed during human diabetic retinopathy. However, we canot ruled out the possibility that hese vessels were persistent hyaloid vessels triggered by the decrease of retinal endostatin in diabetic mice.

Funding

This work was supported by the Instituto de Salud Carlos III, Ministerio de Ciencia e Innovación, Spain (grant number PI16/00719); the Fundação para a Ciência e a Tecnologia, Ministerio da Educação e Ciência, Portugal (grant numbers SFRH/BD/95330/2013 and SFRH/BPD/102573/2014); and Fondo Europeo de Desarrollo Regional (FEDER).

Declaration of competing interest

A. Bonet, None; A. Valença, None; L. Mendes-Jorge, None; A. Casellas, None; A. Rodríguez-Baeza, None; V. Nacher, None; D. Ramos, None; J. Pampalona, None; R. Simó, None; Ruberte, None.

Acknowledgements

The authors thank Lorena Noya, Verónica Melgarejo, and Ángel Vázquez for their technical assistance.

References

Bhutto, I.A., Kim, S.Y., McLeod, D.S., Merges, C., Fukai, N., Olsen, B.R., Lutty, G.A., 2004. Localization of collagen XVIII and the endostatin portion of collagen XVIII in aged human control eyes and eyes with age-related macular degeneration. Invest Ophthalmol Vis Sci 45 (5), 1544–1552. https://doi.org/10.1167/iovs.03-0862.

Bogdanov, P., Corraliza, L., Villena, J.A., Carvalho, A.R., Garcia-Arumí, J., Ramos, D., Ruberte, J., Simó, R., Hernández, C., 2014. The db/db mouse: a useful model for the study of diabetic retinal neurodegeneration. PLoS One 9 (5), e97302. https://doi.org/10.1371/journal.pone.0097302.

Boulton, M.E., Mc Leod, D., Garner, A., 1988. Vasoproliferative retinopathies: clinical, morphogenetic and modulatory aspects. Eye 2, 124–139. https://doi.org/10.1038/eye.1988.139.

Cheung, A.K.H., Fung, M.K.L., Lo, A.C.Y., Lam, T.T.L., So, K.F., Chung, S.S.M., Chung, S. K., 2005. Aldose reductase deficiency prevents diabetes-induced blood-retinal barrier breakdown, apoptosis, and glial reactivation in the retina of db/db mice. Diabetes 54 (11), 3119–3125. https://doi.org/10.2337/diabetes.54.11.3119.

Cristante, E., Liyanage, S.E., Sampson, R.D., Kalargyrou, A., De Rossi, G., Rizzi, M., Hoke, J., Ribeiro, J., Maswood, R.N., Duran, Y., Matsuki, T., Aghaizu, N.D., Luhmann, U.G., Smith, A.J., Ali, R.R., Bainbridge, J.W.B., 2018. Late neuroprogenitors contribute to normal retinal vascular development in a Hif2a-dependent manner. Development 145 (8), 157511. https://doi.org/10.1242/dev.157511.

Deininger, M.H., Fimmen, B.A., Thal, D.R., Schluesener, H.J., Meyermann, R., 2002. Aberrant neuronal and paracellular deposition of endostatin in brains of patients with Alzheimer's disease. J. Neurosci. 22 (24), 10621–10626. https://doi.org/10.1523/JNEUROSCI.22-24-10621.2002.

Ferreras, M., Felbor, U., Lenhard, T., Olsen, B.R., Delaissé, J.M., 2000. Generation and degradation of human endostatin proteins by various proteinases. FEBS Lett. 486 (3), 247–251. https://doi.org/10.1016/s0014-5793(00)02249-3.

Funatsu, H., Yamashita, H., Noma, H., Mochizuki, H., Mimura, T., Ikeda, T., Hori, S., 2003. Outcome of vitreous surgery and the balance between vascular endothelial growth factor and endostatin. Invest. Ophthalmol. Vis. Sci. 44 (3), 1042–1047. https://doi.org/10.1167/iovs.02-0374.

Fukai, N., Eklund, L., Marneros, A.G., Oh, S.P., Keene, D.R., Tamarkin, L., Niemelä, M., Ilves, M., Pihlajaniemi, T., Olsen, B.R., 2002. Lack of collagen XVIII/endostatin results in eye abnormalities. EMBO J. 21 (7), 1535–1544. https://doi.org/10.1093/emboj/21.7.1535.

Hajrasouliha, A.R., Jiang, G., Lu, Q., Lu, H., Kaplan, H.J., Zhang, H.G., Shao, H., 2013. Exosomes from retinal astrocytes contain antiangiogenic components that inhibit laser-induced choroidal neovascularization. J. Biol. Chem. 288 (39), 28058–28067. https://doi.org/10.1074/jbc.M113.470765.

Hanai, J., Dhanabal, M., Karumanchi, S.A., Albanese, C., Waterman, M., Chan, B., Ramchandran, R., Pestell, R., Sukhatme, V.P., 2002. Endostatin causes G1 arrest of endothelial cells through inhibition of cyclin D1. J. Biol. Chem. 277 (19), 16464–16469. https://doi.org/10.1074/jbc.M112274200.

Haverkamp, S., Ghosh, K.K., Hirano, A.A., Wässle, H., 2003. Immunocytochemical description of five bipolar cell types of the mouse retina. J. Comp. Neurol. 455 (4), 463–476. https://doi.org/10.1002/cne.10491.

Hou, Q., Ling, L., Wang, F., Xing, S., Pei, Z., Zeng, J., 2010. Endostatin expression in neurons during the early stage of cerebral ischemia is associated with neuronal apoptotic cell death in adult hypertensive rat model of stroke. Brain Res. 1311, 182–188. https://doi.org/10.1016/j.brainres.2009.11.033.

Huaman, J., Naidoo, M., Zang, X., Ogunwobi, O.O., 2019. Fibronectin regulation of integrin B1 and SLUG in circulating tumor cells. Cells 8 (6), 618. https://doi.org/10.3390/cells8060618.

Hurskainen, M., Eklund, L., Hägg, P., Fruttiger, M., Sormunen, R., Ilves, M., Pihlajaniemi, T., 2005. Abnormal maturation of the retinal vasculature in type XVIII collagen/endostatin deficient mice and changes in retinal glial cells due to lack of collagen types XV and XVIII. FASE J. 19 (11), 1564–1566. https://doi.org/10.1096/fj.04-3101.

Im, E., Venkatakrishnan, A., Kazlauskas, A., 2005. Cathepsin B regulates the intrinsic angiogenic threshold of endothelial cells. Mol. Biol. Cell 16 (8), 3488–3500. https://doi.org/10.1091/mbc.e04-11-1029.

Inoue, S., 1989. Ultrastructure of basement membranes. Int. Rev. Cytol. 117, 57–98. https://doi.org/10.1016/S0074-7696(08)61334-0.

Ito, M., Yoshioka, M., 1999. Regression of the hyaloid vessels and pupillary membrane of the mouse. Anat. Embryol. 200 (4), 403–411. https://doi.org/10.1007/s004290050289.

Kachi, S., Binley, K., Yokoi, K., Umeda, N., Akiyama, H., Muramatu, D., Iqball, S., Kan, S., Naylor, S., Campochiaro, P.A., 2009. Equine infectious anemia viral vector-mediated codelivery of endostatin and angiostatin driven by retinal pigmented epithelium-specific VMD2 promoter inhibits choroidal neovascularization. Hum. Gene Ther. 20 (1), 31–39. https://doi.org/10.1089/hum.2008.046.

Kim, J., Kim, C.S., Lee, I.S., Lee, Y.M., Sohn, E., Jo, K., Kim, J.H., Kim, J.S., 2014. Extract of Litsea japonica ameliorates blood-retinal barrier breakdown in db/db mice. Endocrine 46 (3), 462–469. https://doi.org/10.1007/s12020-013-0085-x.

Kim, Y.M., Jang, J.W., Lee, O.H., Yeon, J., Choi, E.Y., Kim, K.W., Lee, S.T., Kwon, Y.G., 2000. Endostatin inhibits endothelial and tumor cellular invasion by blocking the activation and catalytic activity of matrix metalloproteinase 2. Cancer Res. 60 (19), 5410–5413.

Kim, Y.M., Hwang, S., Kim, Y.M., Pyun, B.J., Kim, T.Y., Lee, S.T., Gho, Y.S., Kwon, Y.G., 2002. Endostatin blocks vascular endothelial growth factor-mediated signaling via direct interaction with KDR/Flk-1. J. Biol. Chem. 277 (31), 27872–27879. https://doi.org/10.1074/jbc.M202771200.

Kishimoto, A., Kimura, S., Nio-Kobayashi, J., Takahashi-Iwanaga, H., Park, A.M., Iwanaga, T., 2018. Histochemical characteristics of regressing vessels in the hyaloid vascular system of neonatal mice: novel implication for vascular atrophy. Exp. Eye Res. 172, 1–9. https://doi.org/10.1016/j.exer.2018.03.024.

Klingeborn, M., Dismuke, W.M., Bowes-Rickman, C., Stamer, W.D., 2017. Roles of exosomes in the normal and diseased eye. Prog. Retin. Eye Res. 59, 158–177. https://doi.org/10.1016/j.preteyeres.2017.04.004.

L'Esperance, F.A., 1998. The Natural History and Classification of Diabetic Retinopathy. Diabetic Renal-Retinal Syndrome. Springer Netherlands, pp. 117–150.

Li, J., Wang, J.J., Yu, Q., Chen, K., Mahadev, K., Zhang, S.X., 2010. Inhibition of reactive oxygen species by lovastatin downregulates vascular endothelial growth factor expression and ameliorates blood-retinal barrier breakdown in db/db mice: role of NADPH oxidase 4. Diabetes 59 (6), 1528–1538. https://doi.org/10.2337/db09-1057.

Li, Y., Li, L., Li, Z., Sheng, J., Zhang, X., Feng, D., Zhang, X., Yin, F., Wang, A., Wang, F., 2016. Tat PTD-Endostatin-RGD: a novel protein with anti-angiogenesis effect in retina via eye drops. Biochim. Biophys. Acta 1860 (10), 2137–2147. https://doi.org/10.1016/j.bbagen.2016.05.031.

Määttä, M., Heljasvaara, R., Pihlajaniemi, T., Uusitalo, M., 2007. Collagen XVIII/endostatin shows a ubiquitous distribution in human ocular tissues and endostatin-containing fragments accumulate in ocular fluid samples. Graefes Arch. Clin. Exp. Ophthalmol. 245 (1), 74–81. https://doi.org/10.1007/s00417-006-0281-y.

May, C.A., Ohlmann, A.V., Hammes, H., Spandau, U.H.M., 2006. Proteins with an endostatin-like domain in a mouse model of oxygen-induced retinopathy. Exp. Eye Res. 82 (2), 341–348. https://doi.org/10.1016/j.exer.2005.07.005.

Marneros, A.G., Keene, D.R., Hansen, U., Fukai, N., Moulton, K., Goletz, P.L., Moiseyev, G., Pawlyk, B.S., Halfter, W., Dong, S., Shibata, M., Li, T., Crouch, R.K., Bruckner, P., Olsen, B.R., 2004. Collagen XVIII/endostatin is essential for vision and retinal pigment epithelial function. EMBO *J* 23 (1), 89–99. https://doi.org/10.1038/sj.emboj.7600014.

Martín-Granado, V., Ortiz-Rivero, S., Carmona, R., Guitiérrez-Herrero, S., Barrera, M., San-Segundo, L., Sequera, C., Perdiguero, P., Lozano, F., Martín-Herrero, F., González-Porras JR., Muñoz-Chápuli, R., Porras, A., Guerrero, C., 2017. C3G promotes a selective release of angiogenic factors from activated mouse platelets to regulate angiogenesis and tumor metastasis. Oncotarget 8 (67), 110994–111011. https://doi.org/10.18632/oncotarget.22339.

McLenachan, S., Magno, A.L., Ramos, D., Catita, J., McMenamin, P.G., Chen, F.K., Rakoczy, E.P., Ruberte, J., 2015. Angiography reveals novel features of the retinal vasculature in healthy and diabetic mice. Exp. Eye Res. 138, 6–21. https://doi.org/10.1016/j.exer.2015.06.023.

Miosge, N., Simniok, T., Sprysch, P., Herken, R., 2003. The collagen type XVIII endostatin domain is co-localized with perlecan in basement membranes in vivo. J. Histochem. Cytochem. 51 (3), 285–296. https://doi.org/10.1177/002215540305100303.

Nawaz, I.M., Rezzola, S., Cancarini, A., Russo, A., Costagliola, C., Semeraro, F., Presta, M., 2019. Human vitreous in proliferative diabetic retinopathy: characterization and translational implications. Prog. Retin. Eye Res. 72, 100756. https://doi.org/10.1016/j.preteyeres.2019.03.002.

Noda, K., Ishida, S., Inoue, M., Obata, K.I., Oguchi, Y., Okada, Y., Ikeda, E., 2003. Production and activation of matrix metalloproteinase-2 in proliferative diabetic retinopathy. Investig. Ophthalmol. Vis. Sci. 44 (5), 2163–2170. https://doi.org/10.1167/iovs.02-0662.

Noma, H., Funatsu, H., Yamashita, H., Kitano, S., Mishima, H.K., Hori, S., 2002. Regulation of angiogenesis in diabetic retinopathy: possible balance between vascular endothelial growth factor and endostatin. Arch. Ophtalmol. 120 (8), 1075–1080. https://doi.org/10.1001/archopht.120.8.1075.

Ohlmann, A.V., Adamek, E., Ohlmann, Andreas, Lütjen-Drecoll, E., 2004. Norrie gene product is necessary for regression of hyaloid vessels. Invest. Ophthalmol. Vis. Sci. 45 (7), 2384–2390. https://doi.org/10.1167/iovs.03-1214.

O'Reilly, M.S., Boehm, T., Shing, Y., Fukai, N., Vasios, G., Lane, W.S., Flynn, E., Birkhead, J.R., Olsen, B.R., Folkman, J., 1997. Endostatin: an endogenous inhibitor of angiogenesis and tumor growth. Cell 88 (2), 277–285. https://doi.org/10.1016/s0092-8674(00)81848-6.

Pehrsson, M., Bager, C.L., Karsdal, M.A., 2019. Chapter 18-Type XVIII Collagen. Biochemistry of Collagens, Laminins and Elastin: Structure, Function and Biomarkers, second ed. Elsevier, Herlev, Denmark, pp. 149–162.

Ramesh, S., Bonshek, R.E., Bishop, P.N., 2004. Immunolocalisation of opticin in the human eye. Br. J. Ophthalmol. 88 (5), 697–702. https://doi.org/10.1136/bjo.2003.031989.

Ritter, M.R., Aguilar, E., Banin, E., Scheppke, L., Uusitalo-Jarvinen, H., Friedlander, M., 2005. Three-dimensional in vivo imaging of the mouse intraocular vasculature

during development and disease. Investig. Ophthalmol. Vis. Sci. 46 (9), 3021–3026. https://doi.org/10.1167/iovs.05-0153.
Robinson, R., Barathi, V.A., Chaurasia, S.S., Wong, T.Y., Kern, T.S., 2012. Update on animal models of diabetic retinopathy: from molecular approaches to mice and higher mammals. Dis Model Mech 5 (4), 444–456. https://doi.org/10.1242/dmm.009597.
Roy, S., Ha, J., Trudeau, K., Beglova, E., 2010. Vascular basement membrane thickening in diabetic retinopathy. Curr. Eye Res. 35 (12), 1045–1056. https://doi.org/10.3109/02713683.2010.514659.
Ruberte, J., Carretero, A., Navarro, M., 2017. Morphological Mouse Phenotyping. Eye and Related Structures. Panamericana, Madrid, pp. 475–520.
Saint-Geniez, M., D'Amore, P.A., 2004. Development and pathology of the hyaloid, choroidal and retinal vasculature. Int. J. Dev. Biol. 48 (8–9), 1045–1058. https://doi.org/10.1387/ijdb.041895ms.
Sertié, A.L., Sossi, V., Camargo, A.A., Zatz, M., Brahe, C., Passos-Buenos, M.R., 2000. Collagen XVIII, containing an endogenous inhibitor of angiogenesis and tumor growth, plays a critical role in the maintenance of retinal structure and in neural tube closure (Knobloch syndrome). Hum. Mol. Genet. 9 (13), 2051–2058. https://doi.org/10.1093/hmg/9.13.2051.
Simó, R., Carrasco, E., Garcia-Ramirez, M., Hernández, C., 2006. Angiogenic and antiangiogenic factors in proliferative diabetic retinopathy. Curr. Diabetes Rev. 2, 71–98. https://doi.org/10.2174/157339906775473671.
Smith, G., McLeod, D., Foreman, D., Boulton, M., 1999. Immunolocalisation of the VEGF receptors FLT-1, KDR, and FLT-4 in diabetic retinopathy. Br. J. Ophthalmol. 83 (4), 486–494. https://doi.org/10.1136/bjo.83.4.486.
Smith, R.S., John, S.W.M., Nishina, P.M., Sundberg, J.P., 2002. Systematic Evaluation of the Mouse Eye: Anatomy, Pathology, and Biomethods, first ed. CRC Press.
Somerville, R.P.T., Oblander, S.A., Apte, S.S., 2003. Matrix metalloproteinases: old dogs with new tricks. Genome Biol. 4 (6), 216. https://doi.org/10.1186/gb-2003-4-6-216.
Takahashi, K., Saishin, Yoshitsugu, Saishin, Yumiko, Lima-Silva, R., Oshima, Y., Oshima, S., Melia, M., Paszkiet, B., Zerby, D., Kadan, M.J., Liau, G., Kaleko, M., Connelly, S., Luo, T., Campochiaro, P.A., 2003. Intraocular expression of endostatin reduces VEGF-induced retinal vascular permeability, neovascularization, and retinal detachment. Faseb. J. 17 (8), 896–898. https://doi.org/10.1096/fj.02-0824fje.
Valsania, P., Warram, J.H., Rand, L.I., Krolewski, A.S., 1993. Different determinants of neovascularization on the optic disc and on the retina in patients with severe nonproliferative diabetic retinopathy. Arch. Ophthalmol. 111 (2), 202–206. https://doi.org/10.1001/archopht.1993.01090020056023.
Waszczykowska, A., Podgórski, M., Waszczykowski, M., Gerlicz-Kowalczuk, Z., Jurowski, P., 2020. Matrix metalloproteinases MMP-2 and MMP-9, their inhibitors TIMP-1 and TIMP-2, vascular endothelial growth factor and sVEGFR-2 as predictive markers of ischemic retinopathy in patients with systemic sclerosis—Case series report. Int. J. Mol. Sci. 21 (22), 8703. https://doi.org/10.3390/ijms21228703.
Weber, J., Peng, H., Rader, C., 2017. From rabbit antibody repertoires to rabbit monoclonal antibodies. Exp. Mol. Med. 49, e305. https://doi.org/10.1038/emm.2017.23.
Wickström, A.S., Alitalo, K., Keski-Oja, J., 2002. Endostatin associates with integrin alpha5beta1 and caveolin-1, and activates Src via a tyrosyl phosphatase-dependent pathway in human endothelial cells. Cancer Res. 62 (19), 5580–5589.
Yamaguchi, N., Anand-Apte, B., Lee, M., Sasaki, T., Fukai, N., Shapirolvo, R., Lowik, Q., Timpl, R., Olsen, B., 1999. Endostatin inhibits VEGF-induced endothelial cell migration and tumor growth independently of zinc binding. EMBO J. 18, 4414–4423. https://doi.org/10.1093/emboj/18.16.4414.
Zhang, C., Gehlbach, P., Gongora, C., Cano, M., Fariss, R., Hose, S., Nath, A., Green, W.R., Goldberg, M.F., Zigler, J.S., Sinha, D., 2005. A potential role for β- and γ-crystallins in the vascular remodeling of the eye. Dev. Dynam. 234 (1), 36–47. https://doi.org/10.1002/dvdy.20494.
Zhang, C., Asnaghi, L., Gongora, C., Patek, B., Hose, S., Ma, B., Fard, M.A., Brako, L., Singh, K., Goldberg, M.F., Handa, J.T., Lo, W.K., Eberhart, C.G., Zigler Jr., J.S., Sinha, D., 2011. A developmental defect in astrocytes inhibits programmed regression of the hyaloid vasculature in the mammalian eye. Eur. J. Cell Biol. 90 (5), 440–448. https://doi.org/10.1016/j.ejcb.2011.01.003.
Zhu, X., Li, A., Brown, B., Weiss, E.R., Osawa, S., Craft, C.M., 2002. Mouse cone arrestin expression pattern: light induced translocation in cone photoreceptors. Mol. Vis. 8, 462–471.
Zudaire, E., Gambardella, L., Kurcz, C., Vermeren, S., 2011. A computational tool for quantitative analysis of vascular networks. PLoS One 6 (11), e27385. https://doi.org/10.1371/journal.pone.0027385.